Investigating the use of LiDAR scanning as a method for the measurement of timber distortion features

---

by

Adam Boney

Submitted in fulfilment of the requirements for the Degree of Master's of Science

School of Engineering

College of Science & Engineering

University of Glasgow

September 2016

then one of you will

prove a shrunk panel, and like green timber warp, warp.

As You Like It (3.3.1574-5)

Acknowledgements

I would like to extend a great deal of thanks and appreciation to my supervisor Dr Karin De Borst. Her insight, guidance and patience were of limitless value throughout this project. Thanks also to Forestry Commission Scotland and the University of Glasgow for funding this project.

Thanks to Professor Chris Pearce for his questions and suggestions in the latter stages of the project. They greatly helped shape the final draft.

Thanks should also be extended to Dr Paul McLean and Corina Convery of the Forestry Commission's Northern Research Station. Appreciation to both for sourcing and providing the necessary materials and equipment and for helping me use them properly. Further gratitude is warranted for allowing principal work to be carried out in the mild month of July. Similar thanks to James Canavan for his help in explaining how things worked.

A pat on the back, if not a full handshake is owed to Maxine. For the rubbish banter.

And thanks to the fam. Obv.

Abstract

Measuring the extent to which a piece of structural timber has distorted at a macroscopic scale is fundamental to assessing its viability as a structural component. From the sawmill to the construction site, as structural timber dries, distortion can render it unsuitable for its intended purposes. This rejection of unusable timber is a considerable source of waste to the timber industry and the wider construction sector. As such, ensuring accurate measurement of distortion is a key step in addressing inefficiencies within timber processing.

Currently, the FRITS frame method is the established approach used to gain an understanding of timber surface profile. The method, while reliable, is dependent upon relatively few measurements taken across a limited area of the overall surface, with a great deal of interpolation required. Further, the process is unavoidably slow and cumbersome, the immobile scanning equipment limiting where and when measurements can be taken and constricting the process as a whole.

This thesis seeks to introduce LiDAR scanning as a new, alternative approach to distortion feature measurement. In its infancy as a measurement technique within timber research, the practicalities of using LiDAR scanning as a measurement method are herein demonstrated, exploiting many of the advantages the technology has over current approaches.

LiDAR scanning creates a much more comprehensive image of a timber

surface, generating input data multiple magnitudes larger than that of the FRITS frame. Set-up and scanning time for LiDAR is also much quicker and more flexible than existing methods. With LiDAR scanning the measurement process is freed from many of the constraints of the FRITS frame and can be done in almost any environment.

For this thesis, surface scans were carried out on seven Sitka spruce samples of dimensions 48.5x102x3000mm using both the FRITS frame and LiDAR scanner. The samples used presented marked levels of distortion and were relatively free from knots. A computational measurement model was created to extract feature measurements from the raw LiDAR data, enabling an assessment of each piece of timber to be carried out in accordance with existing standards. Assessment of distortion features focused primarily on the measurement of twist due to its strong prevalence in spruce and the considerable concern it generates within the construction industry. Additional measurements of surface inclination and bow were also made with each method to further establish LiDAR's credentials as a viable alternative.

Overall, feature measurements as generated by the new LiDAR method compared well with those of the established FRITS method. From these investigations recommendations were made to address inadequacies within existing measurement standards, namely their reliance on generalised and interpretative descriptions of distortion. The potential for further uses of LiDAR scanning within timber researches was also discussed.

List of Figures

List of Tables

List of Symbols

- α, β, γ direction cosine angles
- Δ_i geodesic distance to neighbourhood points
- θ_{ave} average angle of surface inclination
- $d\theta_{ave}$ change in surface inclination
- H distance parameter
- k k-d tree dimensionality
- n neighbourhood size
- $[\mathbf{T}]$ transformation matrix
- w batten deflection measurement in bow
- W_i Gaussian weighting function
- y batten height measurement in twist
- x^R reference x-axis vector
- y^R reference y-axis vector
- z^R reference z-axis vector
- z_i^R orthogonal deviation of neighbourhood point
- z_{ave}^R average orthogonal deviation of all neighbourhood points

Contents

Investigating the use of LiDAR scanning as a method for the measurement of timber distortion features

September 4, 2016

1 Introduction

1.1 Project Background

Macroscopic distortion of structural-grade timber is a source of considerable concern within the timber industry. As a piece of timber is dried its shape can become greatly altered, potentially rendering it unsuitable for use as a structural element. This alteration of shape, and the subsequent rejection of structural timber not fit for final use, generates waste within the industry, both material and financial.

Within the wider field of timber research, much focus has centred on understanding the mechanisms that drive distortion: namely, the material profile

of wood itself (including its moisture content) and the environmental conditions to which the wood is subjected. However, in order to describe how distortion develops, measuring distortion in a meaningful and universal way is an important first step. Accurately describing the shape (and therefore the potential usability) of a timber batten provides a key function to ensuring efficiency within timber selection procedures.

For relatively small scale experiments, the FRITS frame method is currently the established approach in measuring the surface profile of structural timber pieces. Typically, this method relies on a large degree of interpolation between relatively few measurement points across the timber surface to describe its overall shape. It is the purpose of this project to investigate the use of LiDAR scanning as an alternative approach to measuring distortion features of timber.

The considerably greater number of measurement points taken by the LiDAR scanner generates a more comprehensive description of the timber macroscopic profile. In taking measurements across the entire surface area the need for highly interpolative measuring is markedly reduced. Further, LiDAR scanning in this context is considerably quicker than current approaches, with set-up and scan time far shorter than FRITS. The method also allows for measurements to be taken in any environment, the LiDAR scanner being a highly transportable piece of equipment.

LiDAR scanning is a well-established measurement tool in many other fields

and allows for detailed scans to be taken in a variety of environments. This, coupled with the quickness and efficiency of the technology warrants exploration into its applicability within timber distortion measurement.

1.2 Grading and Classification Processes Within the Timber Industry

Strength grading of structural timber consists of visual and machine grading where timber is classified based on assessment of its strength, stiffness and density. Within machine grading, a process of visual override is undertaken to manually reject timber samples that fail a visual inspection. Here, visual override concerns a range of macroscopic features that may influence a piece of timber's structural performance. Obvious signs of obliquity within the sawn timber's profile, in addition to the presence and concentration of macroscopic defects (such as knots and fissures, rot and insect damage), will help determine a batten's final grading [**BS EN 14081-1, 2016**]. Typically, the process of visual override is slow in comparison to mechanised solutions and requires third party certification. By necessity, the gradings given through visual inspections are conservative [**Holland and Reynolds, 2005**].

For detailed assessments, machine grading is used to determine the quality of a given piece of structural timber. Machine grading techniques for structural timber allow for non-destructive assessment of structural performance. Previously, three-point bending equipment was a standard method for non-destructive measurements. More recently, however, three-point bending ma-

chines are being replaced by x-ray scanning and acoustic resonance testing. With X-ray and microwave scanning, it is possible to measure the presence of knots and the slope of the grain: properties relevant not only to quality control but also structural performance and strength grading [**Goldeneye, 2016**]. Laser interferometer scanners can measure resonance frequency of a timber board, enabling accurate, reliable calculation of the timber's modulus of elasticity [**Viscan, 2016**]. Moisture profiles within the wood material can also be studied using Computed Tomography (CT) scanners [**Sandberg and Salin, 2012**].

Concerning surface-related characteristics of timber, laser-based surface scanning techniques allow for precise dimensional measuring of logs and sawn timber pieces, helping to ensure efficient, economic output from the sawmill. A range of commercial scanning equipment exists which can rapidly generate 360° imaging of a piece of timber, including the end surfaces. Output from these detailed scans allows for measurement of annual growth rings, slope of the grain and the position of the pith: key measurements within quality control procedures [**WoodEye, 2016**]. High-end laser-based scanning solutions also exist to provide precise measurement of distorted boards [**Curvescan, 2016**]. These solutions rely on laser triangulation processes, as opposed to LiDAR devices which rely on a time-of-flight approach.

In smaller, bench-top environments analogue means are generally employed to measure macroscopic features. Scaled devices for measurement of bow, spring, cup and twist (see **section 1.3**) allow for reliable measurements with

minimal expense [**Grohmann et al., 2010**].

The investigations of this thesis focus on the potential to develop a middle path in distortion measurement. The use of large-scale scanning equipment within the timber industry provides saw mills with a highly innovative and ever expanding approach to timber grading. However, the scale and expense of such machinery currently prohibits their widespread use in humbler settings, particularly within a research environment. While bench-top techniques using hand-held analogue tools allow for an accessible and inexpensive alternative to distortion measurement, the information gleaned in this way is limited, lacks standardisation, and fails to provide the greater level of detail afforded by industrialised scanning techniques.

As such, an intermediate approach that exploits the detailed measuring capabilities of scanning methods while remaining accessible and practical for small scale testing environments would be a worthwhile addition to the timber research community.

1.3 Feature Measurement Standards - BS EN 1310:1997

Using existing standards for feature measurement of timber, information can be extracted from measurement data sets (be they from FRITS or LiDAR scanning) to assess the distortion of each batten. The current guidelines provide a standard by which to compare output from the existing FRITS method with output from the alternative LiDAR method.

Existing European guidelines on feature measurement of round and sawn timber are contained within BS EN 1310:1997. These list four types of distortion in timber battens: bow, spring, cup and twist. In order for a timber batten to be used successfully as a structural component, the degree to which it has distorted is important. Battens with little or no deviations from a flat, orthogonal shape respond more consistently to external loads, producing a more reliable structural performance than highly deviated battens. Distorted battens can produce difficulties on a construction site in fitting together timber kits and can eventually cause defects in the finished construction, such as squeaking doors and uneven floors. As such, measuring how a batten deviates from an undeformed shape on a macro level provides a partial yet useful insight into a batten's structural integrity and its potential use as a structural, load-bearing member. Figures 1 to 4 depict the characteristics of each distortion type as well as the criteria by which they are measured [**British Standards Institute, 1997**].

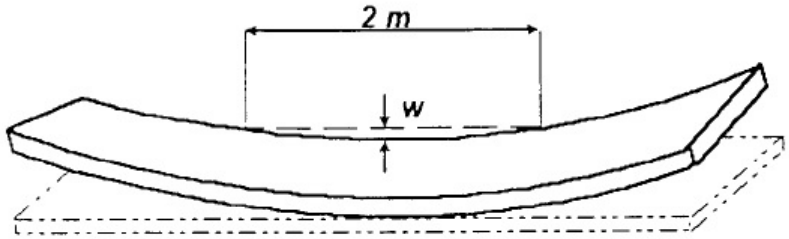

Figure 1: Bow distortion - BS EN 1310:1997 [British Standards, 1997]

Figure 1 shows that 'bow' distortion is characterised by marked curvature along the length of the batten, orthogonal to the batten thickness. 'Spring' is denoted by more prominent bending within the plane of the batten surface. For battens of length greater than 2m, the degree of both 'bow' and 'spring' are given in terms of millimetres per 2m-length.

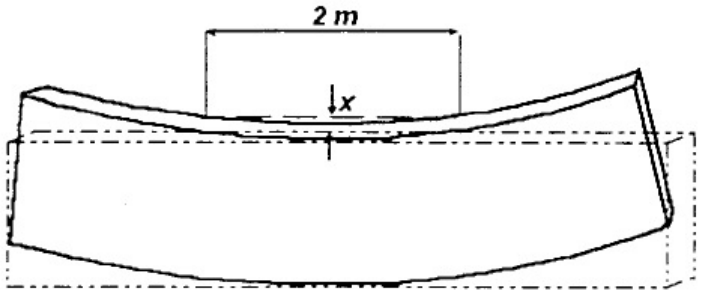

Figure 2: Spring distortion - BS EN 1310:1997 [British Standards, 1997]

With reference to Figure 3, 'cup' considers the lateral cross-section of the batten and expresses deviation as a percentage of batten width. With one lower edge held against a flat surface, 'twist' is measured per width over a length of 2m, with the final distortion measurement given in millimetres per 2m length or as a percentage of the total length.

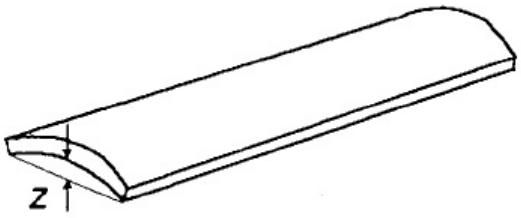

Figure 3: Cup distortion - BS EN 1310:1997 [British Standards, 1997]

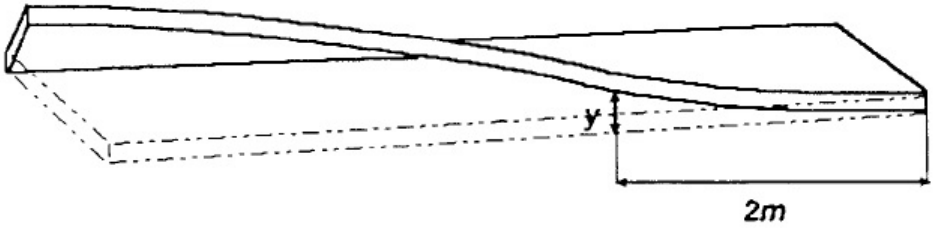

Figure 4: Twist distortion - BS EN 1310:1997 [British Standards, 1997]

These schematics provide insight into the varied nature of batten distortion and highlight the multifarious challenges of working with a highly heterogeneous natural material like wood. The intrinsic material properties of wood and its multiscale nature (each of which is a driving factor in producing these distortions) are covered in the **section 2**.

While the standards provide a workable benchmark by which distortion measurements can be made, they potentially fail to provide an adequate and comprehensive enough approach to feature measurement of timber. For instance, the standards only require measurements to be taken over a 'representative'

2m length as described above, providing no specifications as to what 'representative' may mean for battens of various lengths. Further, limiting the number of distortion features by which a batten can be described to just four may not be exhaustive enough to meet the highly varied nature of timber distortion. These doubts regarding the efficacy and completeness of the standards in part motivate the research carried out here.

Nevertheless, in this project the standards given in BS EN 1310:1997 will serve as a useful reference from which distortion features can be measured. This will allow for standardised comparisons between the existing FRITS technique and the LiDAR approach proposed here, helping validate the accuracy of the new method.

2 Literature Review

2.1 Material Structure of Wood

A thorough approach to measuring the macroscopic deformations of timber must consider the structural and material aspects of wood that underpin the way in which it behaves. As a natural and considerably heterogeneous material whose mechanical profile is greatly influenced by a number of interrelated components operating on multiple length scales, an understanding of timber as a structural material must take an holistic approach in order to ground the research on a firm knowledge base.

Due to its hygrophyllic nature, wood will draw moisture through its porous structure. In broad terms, the presence of water within wood and its movement through the material's heterogeneous substructure leads to discrepancies in how the material reacts during the drying process.

The following overview of wood's material structure briefly traces its salient features from the macroscopic to the molecular scale.

2.1.1 Macrostructure

The salient features of wood macrostructure are largely distinguishable by the naked eye and broadly apply to both hardwood and softwood [**Krabbenhoft, 2003**]. The trunk of the tree serves three main purposes: the support of the crown, the transport of moisture and the storage of necessary nutrients. A cross-section of a softwood log shows two distinct areas. The central

area is the heartwood zone. Encircling this is the sapwood zone [**Frandsen, 2007**]. In Figure 5 the heartwood zone is darker than the sapwood zone. This is not the case for all species, however.

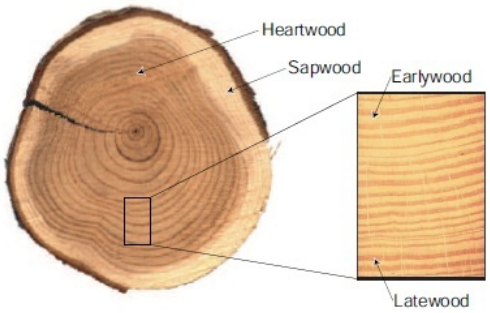

Figure 5: Softwood cross-section [Krabbenhoft, 2003]

A range of characteristic features of wood's macrostructure influence both its mechanical behaviours and shape stability.

With reference to Figure 5, the position from which battens are cut within the log will have an impact on how they distort. Battens cut from the centre of the log, nearest the pith, are more prone to twist [**Johansson and Ormasson, 2009**]. The presence of juvenile wood in the centre of the log is a leading factor in causing this increased twist. This is due to the angle of wood fibres at the centre of the log, which often present greater variability and higher degrees of orientation than the outer portions of the log. Coupled with tangential shrinkage experienced as the board is dried, this variation in wood fibre curvature produces greater internal stresses, increasing the extent

to which the wood distorts at a macro level [**Johansson and Ormasson, 2009; Sandberg, 2005**]. To this end, strategic cutting procedures are required within sawmills to ensure structural timber is cut furthest from the pith.

The way in which a tree grows can greatly influence the material composition (and subsequent mechanical properties) of the timber it yields. Where a tree grows at an orientation or out of equilibrium, reaction wood develops. Reaction wood can be formed by a number of environmental factors, from wind exposure, snow loadings, sloping ground and asymmetries within the tree shape. While the chemical and material changes unique to reaction wood are a necessary adaptation that allows the continued growth of the tree, the timber it yields demonstrates poor mechanical performance [**Du and Yamamoto, 2007**]. In softwoods, where wood material has been subjected to compressive forces (for example, on the underside of a sloping tree or on the leeward side of a tree exposed to strong winds) compression wood forms. Variations within the material profile of compression wood, in particular a higher microfibril angle (see **section 2.1.2**), can greatly impact the wood's future shape stability [**Forestry Commission, 2003**].

Mechanical behaviour of the timber can also be influenced by knots within the wood surface [**Lukacevic et al., 2014**]. Localised distortions of the grain direction are created around the knot, leading to disturbances in stress distributions. The resultant sloping grain around knots can reduce tension strength, compromising a batten's potential structural performance [**New**

Zealand Timber Industry Federation, 2007].

Of further consideration to macroscopic distortion is the influence of the drying process. How the battens are dried and the way in which they are stored and restrained throughout can have an influence on their final morphology [**Johansson, 2006**]. This shows clearly how early on in the milling process a batten's future shape stability can be determined.

2.1.2 Microstructure

On a cellular level, the microstructure of wood comprises an arrangement of longitudinal, approximately square cells known as tracheids. These cells do not follow exactly the direction of the longitudinal axis of the tree, but instead present a spiral or helical orientation, similar to the orientations of the wood grain. This spiral grain angle varies within the stem and is typically no more than 5° [**Neagu et al., 2006**]. Newly formed tracheid cells serve to transport water throughout the tree. Their large cross-section and thin cell walls allow this. As the tree grows, new tracheid cells form to provide structural support. Here, developing tracheid cells display smaller cross-sections and thicker cell walls. The schematic in Figure 6 highlights this arrangement in a softwood tree.

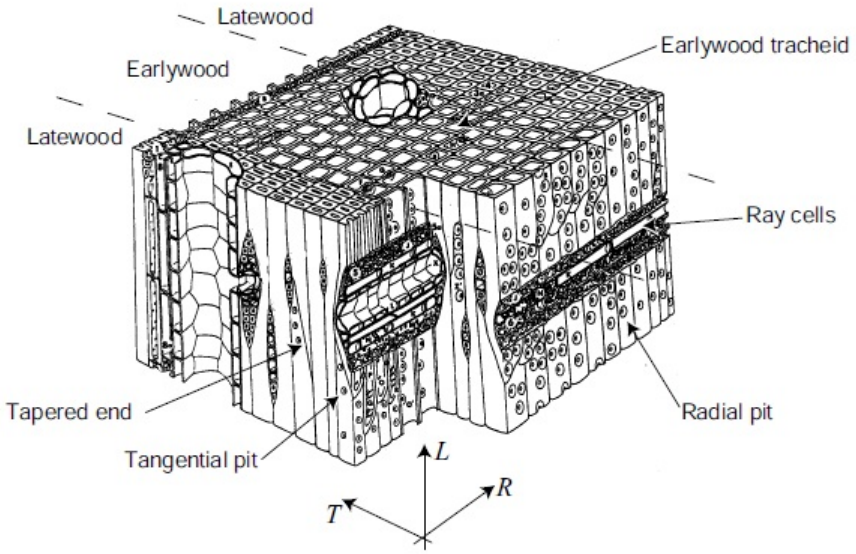

Figure 6: Tracheid arrangment [Krabbenhoft, 2003]

The development of these tracheid cells as the tree grows can have a significant impact on macroscopic distortion. Longitudinal compression of cells creates internal stresses within the wood, as compressed cells pull on adjoining cells. The distribution of these internal stresses will affect how the batten distorts after sawing [**Johansson and Ormasson, 2009**]. The movement of moisture through the cell structure, particularly during the drying process, is also a key factor in generating distortion [**Fransden, 2007**]. Further, the angle of spiral grain contributes significantly to macroscopic distortions. Larger values of spiral grain angle have shown a strong correlation with greater degrees of shape instability, particularly towards the development of twist [**Watt et al., 2013, Ekevad, 2005**].

2.1.3 Ultra-structure

The cell wall of each tracheid comprises a multi-layered structure consisting of a primary wall (P) and a secondary wall (S). This secondary wall is in itself comprised of a number of layers: *S1* = outer layer, *S2* = middle layer and *S3* = inner layer. These are shown in Figure 7. Though the layers differ in terms of thickness and composition, each is constructed from a matrix material reinforced by microfibrils.

Packed tightly together, these thread-like microfibrils constitute the material structure of the cell wall, with each microfibril measuring around 5000nm in length and between 10 and 20nm in width [**Krabbenhoft, 2003**].

The discrepancies between microfibril orientations within the secondary wall provide much of the structural rigidity of the cell wall. The release of internal stresses when the batten is cut from the log plays a key role in generating macroscopic distortion. The readjustment of fibres at this ultrascale, coupled with the movement of moisture through the network of lumens, greatly determines the batten‘s final shape.

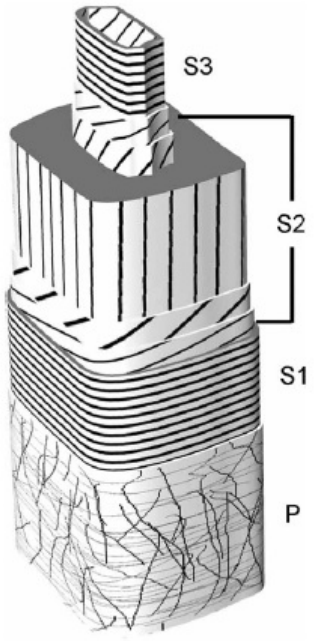

Figure 7: Cell wall schematic [Neagu et al., 2006]

2.1.4 Molecular Structure

On a molecular scale, wood can be considered to comprise of three polymers: cellulose, hemicellulose and lignin [**Neagu et al., 2006**]. Combined, the three polymers form the microfibril structures introduced above, where cellulosic fibrils are embedded within a matrix of hemicellulose and lignin. The cellulose provides the stiff support structure, while it is thought that hemicellulose may act has a bonding agent between the cellulose and lignin [**Neagu, 2006**]. The arrangement of the three polymers within the microfibril structure is shown in Figure 8.

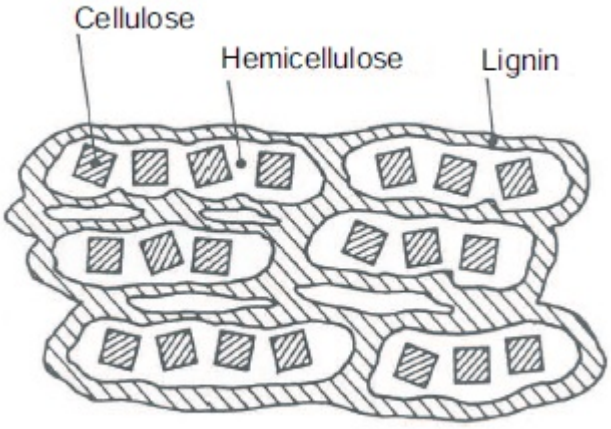

Figure 8: Cross-section of single microfibril [Krabbenhoft, 2003]

This description of the material profile of wood emphasises the interdependent nature of the constituent parts of wood material and the importance of a comprehensive overview of their properties and interactions. In addition to the material of the cell wall structure, the influence and interplay of moisture within the structure is a second key factor in the development of macroscopic deformations.

2.2 Moisture in Wood

As with the material structure of wood, an accurate description of water in wood requires analysis on a number of different levels. In this instance, 'moisture' does not simply mean liquid water. Rather, it encompasses three distinct forms. Here, moisture states are discussed within the context of green timber drying.

2.2.1 Free Water

Typically, free water is found only in living trees and wood in direct contact to water. There is an upper limit to the amount of moisture the fibrous cell wall material can hold. When this limit is exceeded, free water is formed which is then transported through void spaces within the tracheids [**Krabbenhoft, 2003**]. The influence of free water on macroscale mechanical properties of wood is negligible [**Eitelberger, 2011**].

2.2.2 Bound Water

In this form, water molecules which are chemically bonded by intermolecular forces to the wood substance are considered. Linked to fluctuations in relative humidity, changes in bound water concentration bring about volume changes in the cell wall. It is the associated strains and stresses which thus lead to shrinkages and swelling in the macrostructure of the wood [**Eitelberger, 2011**].

2.2.3 Water Vapour

As liquid water begins to dry, it is replaced by a mixture of air and water vapour. This water vapour is particularly difficult to model accurately [**Krabbenhoft, 2003**].

2.2.4 Fibre Saturation Point

The concept of a fibre saturation point becomes pertinent to the discussion of macro-level distortion when we consider that macroscopic deformations only occur at moisture content levels below the FSP. With battens routinely kiln dried to moisture contents of around 18%, the conditions under which deformations are likely to occur will almost certainly be met in most commercial drying processes. Drying freshly cut, green-state timber battens from relatively high moisture content levels to moisture contents sufficiently below the FSP instigates moisture transport mechanisms which create movement and shrinkage across the cell wall material, in turn driving macroscopic changes to the timber batten shape.

Again, by assessing the state and influence of moisture in timber, another layer of interconnectivity is added to the hierarchical nature of wood's material behaviour.

2.3 Summary

As part of an investigation into macroscale distortion measurement, the description of wood as a mutliscale, hygrophyllic and extremely heterogeneous

material presented here is vital to understanding the influencing factors that drive distortion to begin with.

The shape of a distorted timber batten as observed at the macroscale is the result of complex interactions within the wood material across multiple length scales. In addition, the presence and movement of moisture through the wood material will greatly determine the batten's final form.

Wood as a structural material obtains its stiffness from the rigid, densely packed structure of its cell walls. The rigidity of the cell wall is achieved by stiff microfibrils, wrapped in contrasting helical patterns in a number of layers to form the cell wall structure. These microfibrils act together to resist axial and torsional movements. The stiffness of the microfibrils is in turn gained from its matrix composition of polymers: cellulose, hemicellulose and lignin. Cellulose provides much of the structural support to this matrix; however, the interplay between all three polymers ensures support is provided in longitudinal and transverse directions. Upon cutting the timber, the internal stresses of the microfibrils- rooted at the molecular scale- experience a release and begin to pull the cell wall material.

Further, as the timber is dried, a movement of moisture is instigated through the network of lumens within the cell wall as moisture travels from levels of high concentration to low. The anisotropic nature of wood ensures that moisture distribution and movement is not constant across the material. Thus moisture level gradients are created. The presence of moisture in the cell

wall structure (either as bound water or water vapour) causes swelling and shrinkage of the cell wall material. The uneven distribution of moisture will naturally lead to uneven shrinkages and swelling across the cell wall network.

These molecular level movements and interactions eventually scale up, through the material structure described above, to generate movements at the macro level. It is these macroscopic movements that are of interest to this thesis. However, as we have shown, their origin is of a much smaller, more subtle dimension.

Presenting a new method for measuring timber distortion, as is the purpose of this thesis, without consideration to its fundamental causes would leave the work detached from the wider context in which it sits. A macroscopic description of timber distortion features addresses *how* a batten has deformed and to what extent. However, a multiscale understanding of the nature of wood and its properties addresses *why* the batten presents such deformations.

3 FRITS Frame

3.1 Introduction

Developed at Freiburg University, the Freiburg's Improved Timber Scan (FRITS) frame is a terrestrial scanning method for feature measurement of distorted timber battens [**Seeling and Merforth, 2000**].

Figure 9: FRITS frame equipment [Canavan, 2013]

A ‘semi-automated’ method, the FRITS frame comprises a steel frame structure, in which the batten sits, and a set of two lasers. Distortion is measured by one laser measuring vertical displacement at prescribed intervals along the length of the batten, the longitudinal position being logged by the horizontal laser.

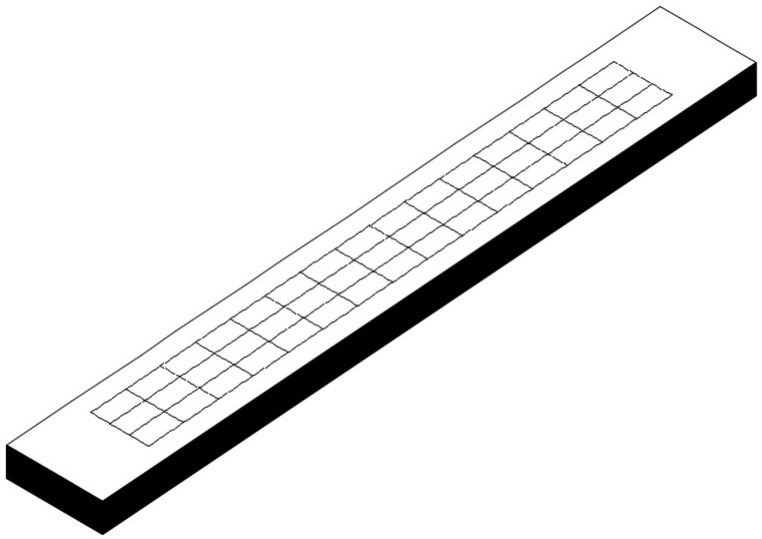

Figure 10: Scan area of batten surface under FRITS frame scanning

Figure 10 shows a typical scan layout for a batten in the FRITS method. A measurement is taken at each intersection point of the scan grid. Note that the scan area does not cover the entirety of the batten surface and that the number of measurements taken is relatively small.

3.2 Feature Measurement with FRITS Frame - Surface Inclination

A description of distortion features is obtained by extracting the relevant measurements taken at various positions along the batten length. For example, the inclination of the batten surface at particular point (or 'slice') can be obtained by interpolating between complementary sets of vertical readings as follows:

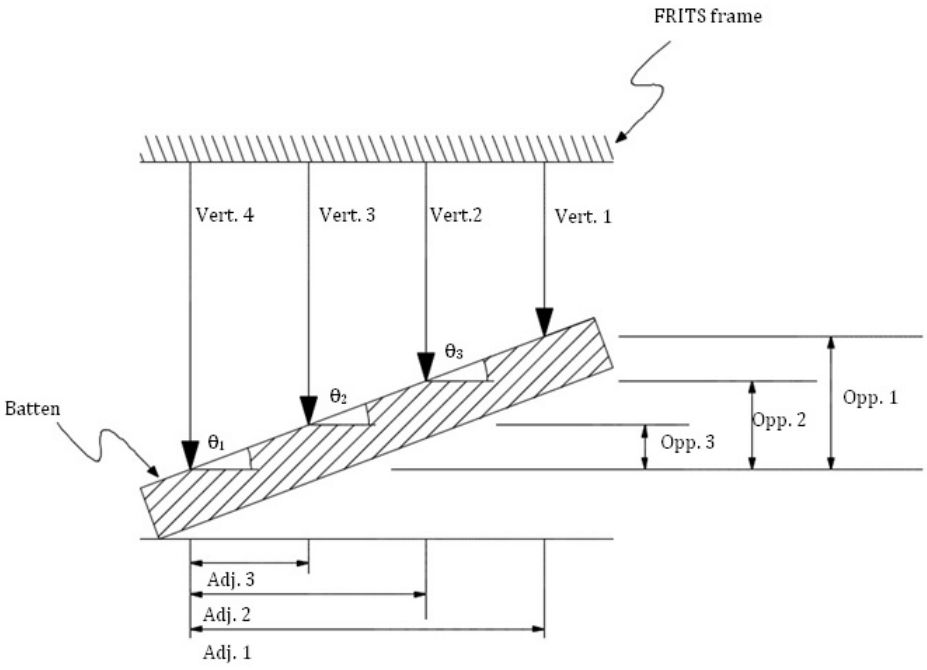

Figure 11: Batten width cross-section on FRITS

$$Opp.1 = Vert.4 - Vert.1 \tag{1}$$

$$Opp.2 = Vert.4 - Vert.2 \tag{2}$$

$$Opp.3 = Vert.4 - Vert.3 \tag{3}$$

Each of the 'Vert.' displacements represents a measurement taken by the vertical laser along the length of the batten. The adjacent values ($Adj.|_{1,2,3}$) are measured manually. The position of these measurements is at the discretion of the user, depending on the size of the scan area and the number of measurement points desired. For a standard 3m long batten of width 100mm, three adjacent lengths of approximately 20mm, measured 20mm in from the batten edge provide a suitably wide scan area, while ensuring all points remain on the batten surface.

From Figure 11, each 'slice' taken with the FRITS frame contains three angles, $\theta|_{1,2,3}$. A linear interpolation is used to calculate an angle of inclination for the 'slice'. Given the relatively short distance between measurements, describing the batten surface by three separate linear interpolations and averaging the results provides a good approximation for the change in surface inclinations. A detailed description of the experiment set-up is given in **section 5.2**.

$$\theta_1 = \tan^{-1}(\frac{Opp.1}{Adj.1}) \tag{4}$$

$$\theta_2 = \tan^{-1}(\frac{Opp.2}{Adj.2}) \tag{5}$$

$$\theta_3 = \tan^{-1}(\frac{Opp.3}{Adj.3}) \tag{6}$$

An average value of angle theta (θ_{ave}) for each 'slice' can be plotted along the length of the batten to provide a picture of how the inclination of the batten changes from one end to the other.

$$\theta_{ave} = \frac{\theta_1 + \theta_2 + \theta_3}{3} \tag{7}$$

The description of batten shape gained by the FRITS method is not limited to these lateral 'slices'. The array of 'Vert.' measurements taken across the surface can be selectively assessed to measure distortion in the various ways described in BS EN1310:1997 (see **section 1.3**).

The FRITS frame is a reliable and proven method for establishing batten distortion, requiring little set-up or expertise. However, it is possible that with the relatively low number of data points along the batten, as well as the necessary interpolation between such few data points, much of the batten surface is missed. As such, smaller, more detailed features may be overlooked or unduly simplified. Further, the method can be laborious and time-consuming, limited to a slow turn around of scans. It is the potential to expand upon the FRITS frame method that will be investigated here.

4 LiDAR Scanner

4.1 Introduction

In this section the nature of LiDAR technology is discussed before introducing a method for using LiDAR scanning to describe the distortion of timber battens. Investigation was undertaken to determine how this new method performs as a practical, reliable alternative measurement technique. Providing a more detailed description of the batten surface, in contrast to the point-wise analysis of the FRITS frame, the use of LiDAR scanning was investigated as an alternative methodology in macroscopic feature analysis.

4.2 LiDAR Technology

Light Detection and Ranging (LiDAR) technology has been used extensively in a number of fields to provide accurate three-dimensional depictions of objects and environments. A standard tool in architectural studies, land surveying and mapping, the technology has seen an increase in its demand and popularity over the last ten years [**Sun and Salvaggio, 2013**]. While technical details may differ from model to model, a LiDAR scanner collects information about its spatial environment by rotating around a fixed point, emitting intermittent beams of light (be it ultra-violet, visible or infra-red) onto surrounding surfaces. The reflected beams of light are processed and

a three-dimensional polar coordinate of each reflected point is stored. The resulting data set, known as a point cloud, comprises a list of these coordinates with no reference to their connectivity or their relationship with one another. The only raw measurement gleaned from the LiDAR scan is the distance from the scanner to the surface off which the laser reflects. It falls to the user as to what post-processing is carried out on the point cloud, depending on the focus of the research or application. This open-ended nature of how scans can be used is very much a key motivator in investigating and validating the use of LiDAR scans in timber research.

Point cloud data returned from these scans benefits from a high level of detail and accuracy, with the resultant images providing a faithful representation of the scan environment. The versatility of scanning equipment, coupled with developments in both scan technology and the software used in post-processing has guided this research into exploring a new, fertile area of inquiry for the timber industry.

4.2.1 LiDAR Scanning - Measurement Method Overview

The method proposed here for distortion measurement aims to utilise the extensive detail gained from the LiDAR scan to describe the distorted surface and compare its performance to more conventional methods.

In essence, the LiDAR scanning method describes a batten surface using the same concept as the FRITS frame method, only with a far greater, more extensive number of sample points. With the FRITS frame, vertical devia-

tion is measured from a fixed datum at selected points across the batten. In each FRITS scan, the datum is set by the frame structure in which the batten sits. In the LiDAR method here, however, the only piece of information obtained from the point cloud is the global coordinates of each of the points. Their connectivity and the shape they describe are unknown at the outset. As such, the first key challenge in this method is to construct a standardised datum for each scan. This datum is called the reference surface and it serves as a benchmark from which distortion measurements are made with LiDAR scanning.

The reference surface is a flat plane described by its own reference coordinate system ($\mathbf{x^R}$, $\mathbf{y^R}$, $\mathbf{z^R}$), independent of the global coordinate system $(\mathbf{x}, \mathbf{y}, \mathbf{z})$ established by the LiDAR scanner (the scanner itself acts as origin to the global scheme). As shown in Figure 12 below, the reference axes ($\mathbf{x^R}$, $\mathbf{y^R}$) are positioned such that their origin is positioned approximately at a batten corner edge, with the $\mathbf{x^R}$ axis approximately aligning with the short edge of the batten; the $\mathbf{y^R}$ axis following the general direction of the long edge. The vectors describing the reference axes are necessarily orthogonal to each other. The reference axes could be positioned anywhere in space; however, this placement convention was the simplest choice.

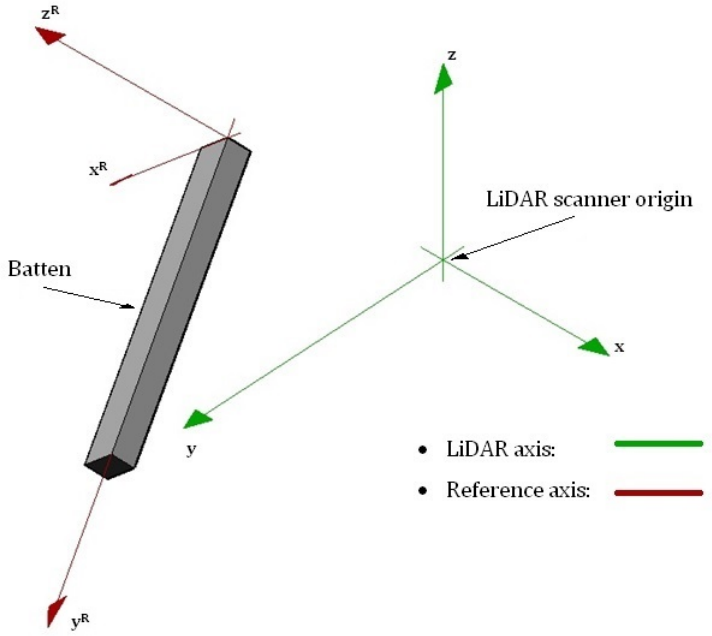

Figure 12: Reference axis placement

By using a transformation matrix consisting of the direction cosines of the reference axis vectors, global coordinates of the point cloud data $(\mathbf{x}, \mathbf{y}, \mathbf{z})$ are rotated into equivalent reference coordinates ($\mathbf{x^R}$, $\mathbf{y^R}$, $\mathbf{z^R}$). The reference $\mathbf{x^R}$ & $\mathbf{y^R}$ values describe the position of each LiDAR point projected onto the reference surface. The reference $\mathbf{z^R}$ value describes the orthogonal deviation of that point to the reference surface: equivalent to the deviation measured by the FRITS.

Following the approximate shape described by the projected points on the reference surface, a grid network, called the reference grid, is established. Each point on the reference grid uses the orthogonal deviations of the near-

est surrounding points on the reference surface to establish an averaged orthogonal deviation value. Thus, each point on the reference grid provides an approximated description of how the batten surface sits in space. It is to the discretion of the user which distortion features are extracted from this data.

4.3 LiDAR Scanning Method Description

4.3.1 Reference Axis Placement

The Cartesian coordinates obtained from LiDAR scans are the only raw data needed to calculate distortion in this method. In order to transform the LiDAR points onto a reference surface, a separate coordinate system must be created, distinct from the x,y,z-axes of the LiDAR scanner. Those edges representing the width and length of the batten are used to position the $\mathbf{x^R}$ and $\mathbf{y^R}$-axes respectively, ensuring that neither axis deviates too greatly from the batten edge while maintaining their necessary orthogonal relationship (This reduces the need for extra spatial translations when projecting points onto the surface). A third axis $\mathbf{z^R}$ is calculated from the cross product of $\mathbf{x^R}$ and $\mathbf{y^R}$. These three vectors are then used to construct a transformation matrix, converting raw LiDAR coordinates into the equivalent reference coordinates.

4.3.2 Sharp Feature Analysis Method

In the initial stages of this investigation, an almost automatic approach to establishing the $\mathbf{x^R}$ and $\mathbf{y^R}$ axes was sought, whereby the reference axes would be created and positioned directly from the raw point cloud data without requiring any initial assessment or calculation. This approach sought to use

existing methods of feature extraction from point cloud data sets, specifically the detection method of 'sharp' features as described by Weber, Hahmann et al [**2010**].

In their approach, information about the position of each point in the cloud is obtained by analysing a 'neighbourhood' of its surrounding points. How the cross-products of consecutive pairs of neighbourhood points vary in their directions provides insight into whether the point under analysis is 'sharp' or 'flat', with sharp and flat points showing marked differences in the way in which cross products are distributed. This type of analysis, described in detail below, would allow one to identify the batten edges within the point cloud and place the reference axes along their appropriate edges as required.

By this method, a k-nearest neighbourhood search is carried out across the point cloud set. This type of classification algorithm uses the surrounding data set to categorize a particular point based on the nearest surrounding points within the data set. Using the Euclidean distances between the point in question and the surrounding set, the point is classified based on a majority of the k-nearest points.

For the model presented here, the point cloud functions as the data set. Each point in the point cloud is considered in turn. Based on its coordinates, open source neighbourhood search tools (described in detail in **section 4.3.7**) establish which of the surrounding points are nearest according to their geodesic distances. Given a chosen value for 'k', the neighbourhood

search selects the k-nearest points and stores them as a vector. This vector is known as the point's neighbourhood.

Each neighbourhood is then considered in turn. Within a neighbourhood, a unit Gauss sphere is created, centred on the point under analysis. A unit Gauss sphere translates the unit normal vector of a point on a surface onto its equivalent position on unit sphere surface. Within these Gauss spheres, sequential pairs of cross products are calculated using the surrounding neighbourhood points. These cross products are projected up onto the unit Gauss sphere surface where their clustering patterns can be analysed.

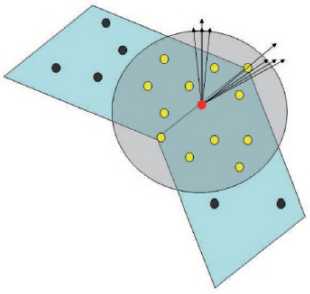

Figure 13: Gauss sphere example [Weber, Hahmann et al, 2010]

In Figure 13, the red point in the centre of the Gauss sphere is the point under analysis. The yellow points are its neighbouring points, i.e. points that are closest to the red point (In this example neighbourhood size, k = 12). The black points fall outwith the neighbourhood and are not included in the calculations.

Depending on where the point under analysis is positioned on the batten surface, the cross products projected onto the Gauss sphere will be distributed in a number of ways. As such, the standard deviation of these distances will markedly change depending on the distribution. The two-dimensional Gauss sphere schematics in Figure 14 highlight three examples of how cross products may be spread on the unit sphere surface.

Figure 14: Two-dimensional Gauss sphere schematics; left-right: flat surface, high curvature, sharp feature [Weber, Hahmann et al, 2010]

With reference to Figure 14, the first case shows a point comfortably positioned on a flat surface. All the points within its neighbourhood lie on the same plane, thus the cross products created all point in the same direction and present a notably concise cluster on the Gauss sphere. As a result of this, the standard deviation of geodesic distances between these points on the Gauss sphere will be low.

The second schematic describes the distribution of a point on an area of high curvature. This particular feature would not be present in scanning rectangular battens, where the shape is adequately described by flat surfaces

and orthogonal edges. Any curvature detected would not be of this high degree. Nevertheless, the method remains the same as above. Now, however, the neighbourhood points no longer lie on the same plane, and the corresponding cross products vary somewhat in their direction. As such, their geodesic distances on the Gauss sphere would have a higher standard deviation than those of a flat surface point.

The last of the examples shows a point on a sharp feature. For points situated on or near an edge, the neighbourhood points will be split between those on one surface on those and those on the adjacent surface. This creates two distinct clusters on the sphere surface. As such, the standard deviation of geodesic distances will be notably higher than those on a flat surface or an area of high curvature.

Considerable investigation was carried out to adopt this approach as the first step in this distortion measurement method. In order to validate the sharp feature analysis code, point cloud sets of cube surfaces with equally spaced points were created. The object here, using simplified and somewhat artificial data, was to confirm that the algorithm worked. Using these test data sets, good results were achieved, with the code successfully identifying those points that described the edges of the cube and dismissing those on the flat surface.

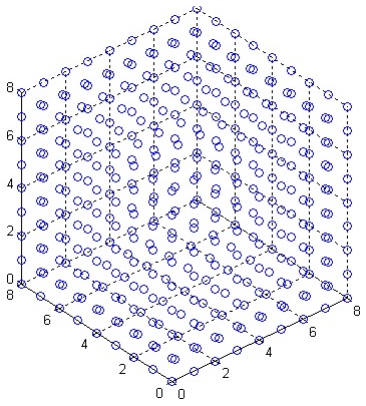

Figure 15: Test cube

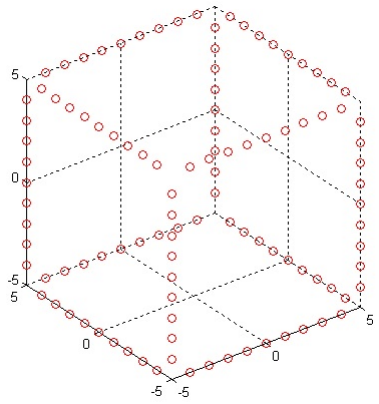

Figure 16: Test cube - sharp feature points

However, when applying this method to more chaotic and rough point cloud data sets from the LiDAR scans themselves, a great deal of difficulty was encountered in identifying sharp features in a reliable way. Some promising results were achieved using low-resolution scans obtained early on in the investigation. The algorithm would successfully identify some points on a

sharp feature, and three-dimensional plots of these points would show perhaps the suggestion of a an edge or a corner. Figure 17 shows the output from the sharp feature algorithm carried out on a corner section of a batten. In this instance, the edges of the top and sides surfaces (shown in red and blue, respectively) were reasonably well identified by the algorithm.

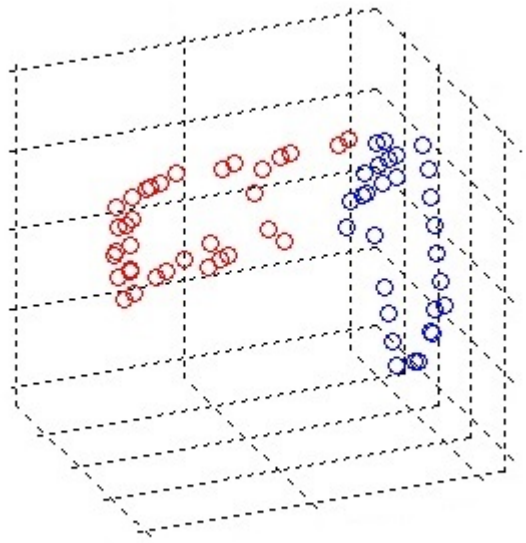

Figure 17: LiDAR data - sharp feature test with batten corner

Nevertheless despite this initially encouraging output, overall the results from the sharp feature algorithm were unclear and unreliable. There appeared to be too much variability between scans and within individual scans themselves to create a reliable, 'universal' method. Assessing the output from these sharp feature analyses, it was found that while some sharp feature

points would be identified correctly, some points were identified incorrectly and others completely missed. Further, in their method Weber, Hahmann et al gave suggested threshold limits for standard deviations to distinguish between the different features shown in Figure 14. These thresholds did not work well with scans used in this project and attempts to establish workable limits produced too much variability from scan to scan. Ultimately, the method proved unsuitable for this project

4.3.3 Direct Vector Placement Method

Following this, a simpler, more direct approach was adopted instead. Here, vectors for the $\mathbf{x^R}$ and $\mathbf{y^R}$-axes were created by assessing the point cloud set 'by hand'; i.e. by manually selecting representative points to describe the short and long edges, positioning the reference axes (and the reference origin) in the necessary place. In this approach, the vectors for both $\mathbf{x^R}$ and $\mathbf{y^R}$-axes were each described by two points (where the vector begun and where it ended), both vectors sharing a common point, the origin of the reference axis system at the batten corner. Slight alternations to the exact coordinates of the selected points were needed to ensure both vectors were orthogonal. These alterations were as minimal as possible in order to avoid any unnecessary spatial translations in the coordinate transformation. Having calculated the $\mathbf{x^R}$ and $\mathbf{y^R}$ vectors it was a simple next step to calculate the corresponding $\mathbf{z^R}$-axis vector from the cross product of $\mathbf{x^R}$ & $\mathbf{y^R}$.

While this method lacks the elegance of the more hands-free, automatic approach initially sought, it effectively and efficiently provides a solution to the

initial step in the distortion measurement code, creating a 'best fit' description of the batten edge as required.

Having established the reference axes in order to carry out a coordinate transformation from the global system to the reference system, the origins of both the global LiDAR coordinate system and the reference coordinate system must be aligned. This is achieved simply by translating the reference origin from its position in space to a value of (0, 0, 0), and translating the $\mathbf{x^R}$, $\mathbf{y^R}$ & $\mathbf{z^R}$-axes accordingly. These translated vectors are then used to calculate direction cosines.

4.3.4 Direction Cosine Angles & Transformation Matrix

The reference axis is defined by the following notation:

$$\mathbf{x^R} = [X_x, Y_x, Z_x] \tag{8}$$

$$\mathbf{y^R} = [X_y, Y_y, Z_y] \tag{9}$$

$$\mathbf{z^R} = [X_z, Y_z, Z_z] \tag{10}$$

For each of these vectors, the three direction cosine angles, α, β and γ, can be calculated to construct a transformation matrix.

$$[\mathbf{T}] = \begin{pmatrix} cos\alpha_x & cos\alpha_y & cos\alpha_z \\ cos\beta_x & cos\beta_y & cos\beta_z \\ cos\gamma_x & cos\gamma_y & cos\gamma_z \end{pmatrix} \tag{11}$$

Where for a generic vector $[a, b, c]$ direction cosine angles are given as:

$$cos\alpha = \frac{a}{\sqrt{a^2 + b^2 + c^2}} \tag{12}$$

$$cos\beta = \frac{b}{\sqrt{a^2 + b^2 + c^2}} \tag{13}$$

$$cos\gamma = \frac{c}{\sqrt{a^2 + b^2 + c^2}} \tag{14}$$

These three angles are calculated for each of the three reference axis vectors.

The transformation from global LiDAR coordinates $[X, Y, Z]$ to equivalent reference coordinates $[X^R, Y^R, Z^R]$, is given as:

$$\begin{pmatrix} \mathbf{x^R} \\ \mathbf{y^R} \\ \mathbf{z^R} \end{pmatrix} = [\mathbf{T}]. \begin{pmatrix} X \\ Y \\ Z \end{pmatrix} - \begin{pmatrix} X_0 \\ Y_0 \\ Z_0 \end{pmatrix} \tag{15}$$

Where vector $[X_0, Y_0, Z_0]$ represents the spatial translation required to match the origins of both coordinate systems.

4.3.5 Point Translation & Reference Surface

The convention adopted here of positioning the $\mathbf{x^R}$ and $\mathbf{y^R}$-axes along the short and long sides of the batten respectively meant that the flat reference surface onto which the LiDAR points are projected is naturally described

on an x-y plane, with the z-component describing the orthogonal distance through which that point has been projected. Note too in this convention that a positive z-component describes a point *above* the reference x-y surface, while a negative z-component describes a point *below* the reference x-y surface. A reference grid is built across these projected x-y reference points.

4.3.6 Reference Grid

The concept of a reference grid across which spatial measurements can be extracted is a salient part of this approach to distortion measurement. The method of constructing the reference grid presented here, however, evolved as the investigations progressed.

Before scans had been carried out, it was assumed that a regular rectangular grid of a comparable size to the batten surface would suffice for this purpose. However, the somewhat varied nature of the batten shapes meant that this generic approach was not wholly applicable. Some battens presented marked lateral distortion, their surfaces curving outwards from the central axis. As a consequence of the projected surfaces curving in the $\mathbf{x^R}$ direction, a regularly spaced rectangular grid would not sufficiently represent the projected surface. These variations in batten shape necessitated a more flexible approach to constructing each reference grid.

The solution decided upon ensured that the number of points comprising the reference grid (the 'resolution' of the grid) remained the same for each scan. Spacing of these points in both the $\mathbf{x^R}$ and $\mathbf{y^R}$ directions was also

identical for each scan. In order to adapt each grid to the projected surface, however, each row of the reference grid began at the left most edge of the projected surface as shown in Figure 18 below. Thus, as each new row of the reference grid was added, a new starting position on the $\mathbf{x^R}$-axis is determined. From this, points are then spaced out at regular intervals to cover the width of the batten [Note: it is assumed the lateral dimensions across the batten do not change along its length. Though the batten may distort, a rigid body movement in both the lateral and longitudinal directions is assumed throughout]. Each row of the reference grid was constructed in this way, with spacing between rows in the $\mathbf{y^R}$ direction being fixed throughout. The reference grids were of resolution 10X50, giving five-hundred points of measurement across the batten surface.

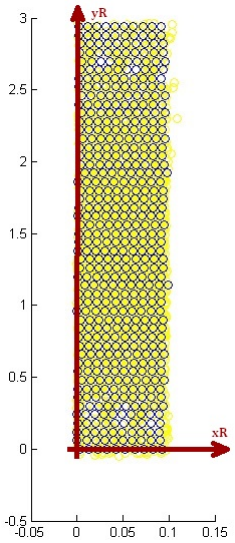

Figure 18: Sample reference grid - batten 2

Batten 2 as shown in Figure 18 provides a typical example of a distorted surface. The reference grid points (coloured dark blue in the figure) follow the slight irregularities of the reference surface points (shown in yellow), giving a closer approximation of the necessary shape.

4.3.7 k-Nearest Neighbour Search & Measurement Extraction

From each point within the reference grid, $\mathbf{z^R}$-coordinate values from the surrounding surface points were collated to create a picture of the spatial profile of the batten. Using open-source neighbourhood search tools developed by Tagliasacchi, a k-nearest neighbourhood of reference surface points is created for each point in the reference grid [**Tagliasacchi, 2010**].

The k-nearest neighbour search algorithm used first organises the data set (in this instance the LiDAR coordinates) into a k-d tree. The k-d tree is a data structuring method that employs binary space partitioning to recursively split the feature space into smaller hyper-regions, generating a tree-like structure in which the original data series is stored [**Moore, 1991**].

To help ensure a relatively balanced tree structure, the algorithm performs median splits for each partitioning sequence. The algorithm selects the median value of all data points within the attribute under consideration. In this instance, there are three attributes by which each data point is defined: its x-, y- and z-coordinates. The median-splitting strategy is facilitated by employing the Heapsort algorithm to sort the data points from least to greatest value for each of the attributes.

In the problem outlined here, dimensionality of the tree is $k = 3$. As such, the algorithm cycles through the three attributes of the data series points (x-, y- and z-coordinates) on each successive partitioning. Moore states that for uniformly distributed data sets, this median splitting strategy works well. However, difficulties can arise when the data sets are non-uniformly distributed [**Moore, 1991**]. The point cloud data sets used in this thesis were all of sufficient resolution to ensure they described a uniform distribution across the batten surfaces.

With the k-d tree structure in place, calculation of the nearest neighbouring points to a query point can be undertaken. This is done by comparing the attributes of the query point to those values presented at each node within the tree. The search algorithm follows the path down the appropriate branches of the tree until those points approximating the query point the closest are found. The Tagliasacchi algorithm provides flexibility in stipulating the number and value of query points chosen. In the model given here, each point in the reference grid represents a query point. In addition, the number of neighbours ('k') is left to the discretion of the user. When the requisite number of neighbours is found, the search stops accordingly.

From these calculations a two-dimensional array can be built in which the indexes of the neighbouring points for every reference grid point are stored. As stated in **section 4.3**, the orthogonal deviation in the $\mathbf{z^R}$ direction describes the position of the batten surface relative to the datum established

by the reference surface. Using the $\mathbf{z^R}$ values for points corresponding to the neighbourhood indexes, an average orthogonal deviation can be calculated for each of the reference grid points using the following expression:

$$z_{ave} = \frac{\sum_{i=1}^{n}(\frac{z_i^R}{\Delta_i})}{\sum_{i=1}^{n}(\frac{1}{\Delta_i})} \tag{16}$$

Where:

n = neighbourhood size

z_i^R = orthogonal deviations of neighbourhood points

Δ_i = geodesic distance to neighbourhood points

The weighted averaging approach used in Equation 16 whereby distance is used as the controlling metric was an intuitive choice given that the k-nearest neighbour search was itself distance-weighted. Each neighbourhood vector was generated based solely on the spatial proximity of LiDAR scan points to reference grid points. As such, it was a natural progression when calculating a weighted average value of orthogonal deviation (z_{ave}) that spatial distance be the controlling variable. However, a number of other distribution functions exist that could be used to carry out a weighted averaging of orthogonal deviations. In **section 7.3**, a comparison is carried out showing the impact of using a generalised Gaussian function as an alternative to the weighted average in Equation 16.

A neighbourhood size of ten was used throughout. This gave good coverage around each grid point and did not produce long run times.

Having established an averaged orthogonal deviation for each point on the reference grid, a profile of how the batten has deformed can be extracted. By analysing specific groups of deviations and tracking their change along the batten length (or width), existing feature measurement standards can be applied to build a description of the batten's distorted shape. The results of these calculations are presented in **sections 6** where three distortion features (surface inclination, twist and bow) were calculated using both the FRITS method and the LiDAR method developed here.

4.4 Alternative Approach To Feature Extraction from Point Cloud Data Utilising Quadratic Surfaces

Fitting surfaces to describe point cloud data sets has been the focus of many and diverse areas of research [**Levin, 2004**]. The preceding section has presented one approach to achieving this. Naturally, many alternative methods exist. To provide a wider context to the solution presented in this thesis, here we highlight an alternative approach to the feature extraction problem.

4.4.1 Quadratic Surfaces

While the distortions that a timber batten can undergo are varied, the final shape that their surfaces describe can be thought of as an originally rectilinear plane that has been curved and warped within three-dimensional space.

As such, the distorted surface to be measured can be approximated by a quadratic surface. In a general form, quadratic surfaces are defined by the equation:

$$Ax^2 + By^2 + Cz^2 + Dxy + Exz + Fyz + Hx + Iy + Jz + K = 0 \qquad (17)$$

where coefficients $A - J$ are fixed, real constants.

In a simplified example, for a batten presenting low levels of twist but marked levels of bow, the surface could be approximated by a parabolic cylinder of the form:

$$By^2 + Jz = 0 \qquad (18)$$

An indicative plot of a parabolic cylinder is shown below. Correctly scaled, such a quadric surface shows the recognisable features of a bowed timber batten (See Figure 1).

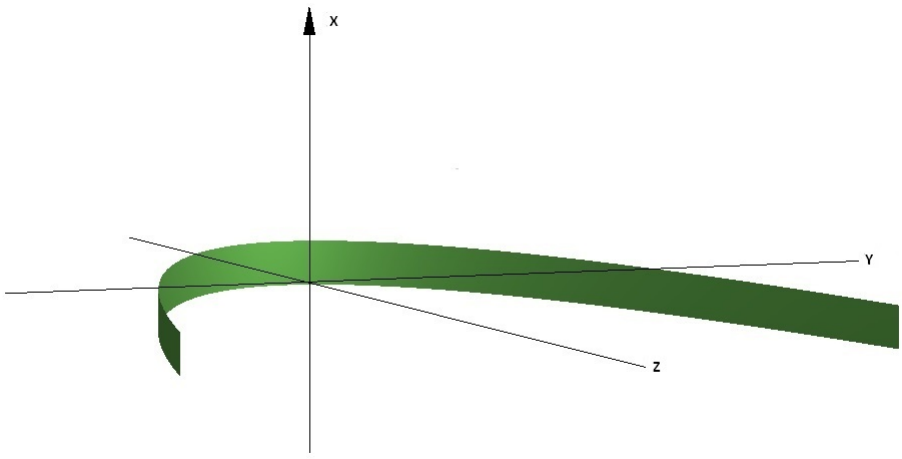

Figure 19: Parabolic cylinder

In order to establish the parameters of Equation (17) and thus define the batten surface, a least squares approximation method could be employed.

4.4.2 Weighted Least Squares Approximation

A least squares approximation seeks to describe a point-wise data set by an alternative reference plane such that the sum of squared distances between the original data set points and the new reference plane is minimised. Minimising the distances through which data set points are projected reduces the error of the final approximated plane. With a localised weighted least squares approximation, the error is typically weighted by a function of the Euclidean distances between the data set points and projected points.

Briefly, let the the point data set be defined by N number of points positioned at x_i, in three-dimensional real space where $i \in [1...N]$. Each point at fx_i is defined by f_i. Function $f(x)$ is defined such that the sum of the squared distances between x_i and $f(x)$. However, with a weighted least squares approach, these distances are weighted by function $\theta(d_i)$, where d_i is the Euclidean distance between x and projected point x_i. The minimisation is given as:

$$\sum_{i=1}^{N} \theta(d)||fx_i - f_i||^2 \tag{19}$$

Weighting function θ can be defined in a number of ways; for example, as a Gaussian: $\theta = e^{-\frac{d^2}{h^2}}$ (see **section 7.3**).

Function $f(x)$ can be written as:

$$f(x) = b(x)^T.c = b(x).c \tag{20}$$

where the basis vector $b(x)$ describes the polynomial of the quadratic surface describing the batten shape, and c is a vector containing the unknown coefficients to be minimised. Taking the partial derivatives of $||fx_i - f_i||^2$ results in a linear system of equations describing the quadratic surface. In order to evaluate curvatures of the surface, the linear system of equations can be standardised in its canonical form.

4.4.3 Canonical Form

Describing the polynomial of the quadratic surface in its canonical form helps to translate the coordinates of the surface points from a global coordinate system to a local, canonical coordinate system - equivalent to the reference coordinate system described in this section - independently of the user, removing the need for subjective selection of data points in determining the reference coordinate system. From here, specific curvatures of the surface can be calculated, allowing for assessment of the batten surface in accordance with feature measurement standards.

5 Experiment Method Description

5.1 Introduction

The scanning experiments focused on comparing distortion measurement using two different techniques. Seven Sitka spruce battens of dimensions 48.5x102x3000mm were used in total. These were sourced from the BSW Timber Group's Carlisle mill. All of the battens had undergone extensive kiln drying at the Forestry Commission's Northern Research Station in Roslyn. Drying was carried out under restrained conditions where each batten had been secured within a bracket and dried progressively over a number of weeks to a moisture content of around 12%. Dried in this way, as part of a separate experiment carried out by colleagues from the University of Glasgow, many of the battens presented with a variety of marked distortion. Selecting battens with clear signs of macroscopic distortion provided a more rigorous test of the new method. All of the test samples were relatively free from knots and indentations.

5.2 FRITS Experiments

A surface scan of each batten was first carried out using the FRITS frame. Each batten was scanned lengthwise four times, each scan comprising fifteen measurements at lengthwise intervals of approximately 0.2m, describing the surface with sixty data points. This interval length matches that which was used by Seeling and Merforth [**2000**] in their initial experiments with their FRITS frame apparatus.

A minimum of two runs is needed to acquire any meaningful results from the FRITS frame as tracing a single line along the batten provides no opportunity to interpolate between results to explain the surface shape. Taking four scans along the batten surface created a measurement area comparable to the overall width of the surface itself. Dividing this area into four measurements of vertical displacement allowed for a comprehensive averaging of the overall batten slope. A higher number of measurements would have provided more input data over which to average. However, given the cumbersome nature of the FRITS frame equipment, this would have proved very time consuming. As such, four lengthwise scans were deemed an appropriate number to work with.

The lengthwise measurement intervals of 0.2m were approximate to around 1/1000m. These discrepancies were largely due to vibrations and jolting produced by the scanner as the vertical laser rig moved along its rail. The stopping mechanism for the vertical laser can be altered manually to create shorter or longer distances between measurements, however, as stated previously, early experiments in establishing the FRITS frame's competence worked with this standard of 0.2m producing reliable, reproducible results [**Seeling and Merforth, 2000**].

For ease of comparison between FRITS frame and LiDAR scans, it was useful to denote one end of the batten as the 'top' (the end at which FRITS measurement were begun) and the other end as 'bottom' (the end at which FRITS measurements finished). This was then taken into consideration when

carrying out LiDAR scans, as described below.

Another practical consideration when using the FRITS frame was to ensure that the batten remained in place while each scan was undertaken. Some jolting and shuddering of the apparatus was observed during tests. This did not appear to cause any problems with the final results. However, given the deformed shape of most of the battens, there was a noted tendency for them to wobble when placed on the flat supports of the frame. Ensuring that each batten was placed firmly against the frame, resting on two points of support along its length was crucial to obtaining consistent, coherent results.

Figure 20: FRITS frame scanning experiment set-up

5.3 LiDAR Experiments

The LiDAR experiments covered in this thesis were carried out using a *FARO Photon 20/120 Laser Scanner*. Commercial laser scanners allow for scans to be made over a range of resolutions, with higher resolutions creating larger point cloud data samples, thus yielding more detailed depictions of the scanning environment. Increasing the sample size naturally lengthens the scan time.

In addition to the resolution setting, the spatial limits, both horizontal and vertical, within which a scan is carried out, must be specified prior to scanning. These limits, or angular area of the scan, again are at the discretion of the user, depending on the environment being scanned and the nature of the investigation. An almost complete 360° scan is possible ('Almost' due to the inability of the scanner to point completely 180° downwards towards the ground).

Although requiring a somewhat longer set-up than the FRITS frame, scanning each of the battens with the LiDAR scanner was a comparatively quicker process. While a full FRITS frame would take six to eight minutes, typically a single LiDAR scan was completed within two minutes.

Selecting a suitable scan resolution was a necessary first step that required balancing the need for an accurate, detailed description of the battens while ensuring practical scan times and workable data sets. An extremely high resolution scan may yield a very accurate point cloud reconstruction of the

batten surface. However, the necessarily long time taken to carry out such a scan, coupled with the large computational burden of analysing the considerable point cloud would not produce a viable, practical solution. Similarly, while a low resolution scan would allow for comparatively quick scans to be taken, and the computational load would be relatively minimal, the point cloud and its resultant analysis would not necessarily provide an accurate or meaningful picture of batten distortion. Experimenting with varying scan resolutions, a mid-range resolution, as described in the manufacturer's literature, provided the best solution. At this resolution, the size of each point cloud was approximately thirty-thousand points. These point cloud sets provided good descriptions of the batten surfaces and edges, while ensuring relatively low computational times.

In order to streamline the process further, the size of the scan window ('angular area') was limited such that a full view of the batten was achieved while much of the surrounding environment was ignored. Creating this slim scan window ensured the number of unnecessary points captured in the scan (i.e. those points that described anything other than the batten surface) where minimised, reducing both the scan time and the amount of post-processing needed to remove unwanted points in the point cloud.

Many of the practical aspects of working with LiDAR scanners are covered in **section 7.1**. For these experiments, it was essential to have an uninterrupted view of the batten surface for each scan. This was easily accomplished by propping up each batten (by its 'top' end) against the rafter of the work shed

in which the experiments took place. This approach only concerns scanning one surface of a batten. It is possible, however, using a LiDAR scanner to achieve a full 360° description of the batten by combining multiple scans taken from several positions around it. By suspending one end of the batten from a rafter, and resting the other end on the floor, a clear passage can be created for the LiDAR scanner to cover all sides of the batten. The spherical targets shown in Figure 21 are used to establish the spatial relationship between multiple scans, describing the position of each scan in relation to the others. This enables the user to combine multiple scans of the same object together to create a complete model. This project only considered the measurement of one surface per batten, however, expanding measurements to an entire batten is a possible avenue of future work (**See section 8.2**).

Figure 21: LiDAR scanning experiment set-up

5.3.1 Comparison to FRITS Frame

Similar to the FRITS frame, spatial deviations measured by the LiDAR scanner in this method can be assessed in a variety of ways to describe the batten shape, in accordance with the standards set out in BS EN1310:1997.

As an example, analysing each row of the reference grid provides horizontal 'slices' across the batten, describing the overall inclination of the batten surface by which an average angle (θ_{ave}) can be calculated. This value can be plotted along the length of the batten, providing a highly detailed description of batten surface deviation along its entire length. This result can then be compared to the traditional FRITS frame approach to assess the suitability of the LiDAR method.

6 Results

6.1 Introduction

Section 1.3 introduced standards BS EN 1310:1997 by which distortion features can be measured in timber battens. For this project parts of the spatial data obtained from both measurement techniques (FRITS and LiDAR) were extracted to allow for comparisons between three measurements of distortion for each batten.

The first of these measurements, not given in the European Standards, is a measure of surface inclination along the length of the batten. This is a standard measurement taken by the FRITS frame and was covered in **section 3.2**. The methodology of FRITS frame measurement, whereby lateral 'slices' are taken at regular intervals along a batten length, leads quite naturally to the measurement of surface inclination (θ_{ave}). With the LiDAR approach presented here, measuring lateral 'slices' along the batten from each row of the reference grid allows for a straightforward comparison with the FRITS method.

Measuring how the angle of the batten surface changes along its length in this way provides an immediate indication of how the surface alters as a whole. The angle measurements here can dovetail into more specific measurements of twist as given in the standards. For example, the instance where θ_{ave} shows little or no change over a considerable length, i.e. the slope of the surface remains on a level plane, would indicate a relatively low or negligible

degree of twist in the batten.

It should also be noted that for the comparison of FRITS and LiDAR measurements, the focus is on the *change* in θ_{ave} along the length of the batten. Both methods describe distortion by measuring orthogonal deviation from points on the batten surface to a prescribed datum. With the LiDAR method presented in this thesis, the datum is set by the placement of the reference axis, which in itself is unique to each scan. This stands in contrast to the fixed datum of the FRITS frame approach and would naturally create orthogonal measurements of different magnitudes. As such, values of θ_{ave} for each 'slice' would differ between both methods. Nevertheless, with both approaches, one would expect the overall trend in θ_{ave} to be the same or similar, providing both methods are consistent within themselves.

The second measurement is that of twist as described in BS EN 1310:1997 over a length of approximately two metres. The European standards for timber feature measurement currently lack clarity and are open to various interpretations of how measurements from a batten should be taken. With specific reference to twist, the standards only advise measuring orthogonal deviation over a 'representative' two metre length (or the length of the piece).

By the FRITS frame scanning convention shown in Figure 22 the vertical measurements along lengthwise scans 'Right' and 'Left' were used to calculate twist in accordance with standards. Each batten was rested on the FRITS frame supports along its 'Right' side as level and as securely as possi-

ble. Measurements of deviation along the outer 'Left' scan length were made relative to the inner 'Right' scan length measurements. From Figure 22, the distance between 'Right' and 'Left' is approximate to the overall width of the batten as required by the measurement standard for twist.

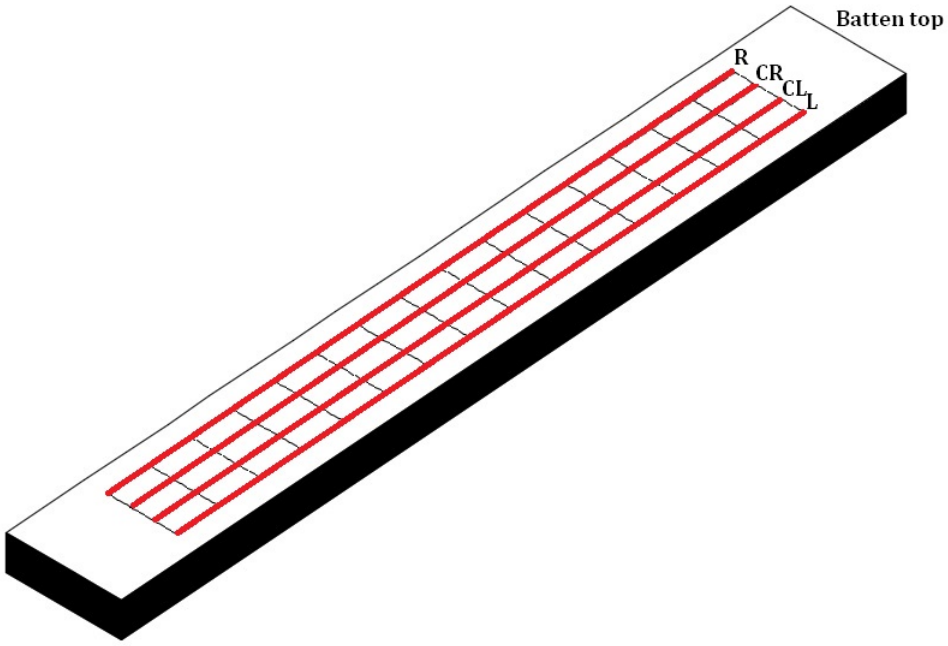

Figure 22: Surface layout of batten measurements for FRITS frame

Using comparable points on each reference grid, this extraction of lengthwise measurements was replicated with the LiDAR method. These values of lengthwise orthogonal deviation can be used to extract a single value of twist

using the approach set out in the standards. With reference to Figure 23, twist is calculated as follows:

$$Twist(\%) = \frac{y}{width} \times 100\% \tag{21}$$

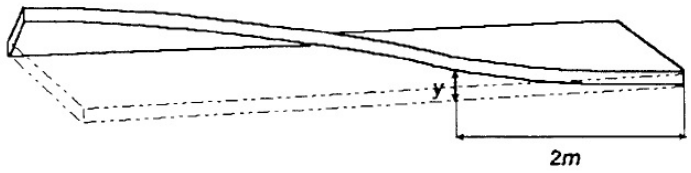

Figure 23: Twist distortion - BS EN 1310:1997 [British Standards, 1997]

The last measurement is that of bow as described in BS EN 1310:1997. Here, bow is measured as the maximum deviation on the concave face along a 2m-length of the batten.

For both FRITS and LiDAR methods, it is a relatively simple process to extract the relevant measurements and assess the maximum value along a 2m-length to give a value for bow. In the case of FRITS, these are the 'Vert' distances; with LiDAR it is orthogonal deviations. Key to generating a valid comparison between both methods is to ensure the same 2m-length is considered. In this instance, bow was measured along the 'Right' length scan on FRITS, beginning approximately 0.4m in from the short edge. Within the LiDAR data, the rightmost length of the reference grid was utilised, beginning the 2m-length at approximately 0.4m in from the short end.

In accordance with European Standards, bow is calculated as follows:

$$Bow(mm/2m) = \frac{w_{max}}{2m} \tag{22}$$

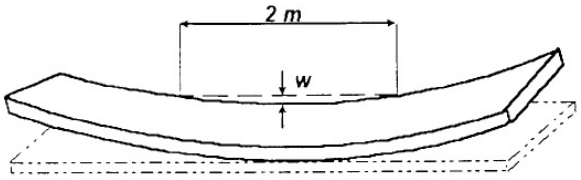

Figure 24: Bow distortion - BS EN 1310:1997 [British Standards, 1997]

6.2 Change in Surface Inclination Measurements

6.2.1 Average Theta Plots

The value of θ_{ave} (defined in **section 3.2**) as measured by FRITS and LiDAR methods is plotted against a two-metre length for each of the seven battens. These plots show the extent to which the batten surfaces deviate from the datum established by each measurement technique. A measured value of θ_{ave} = 0 denotes a portion of the batten which lies in plane with the datum. A linear trend line of each of these plot is used to calculate change in θ_{ave}, thus facilitating a comparison between FRITS and LiDAR measurements shown in Table 1. A full discussion of these results is presented in **section 7.2.1**.

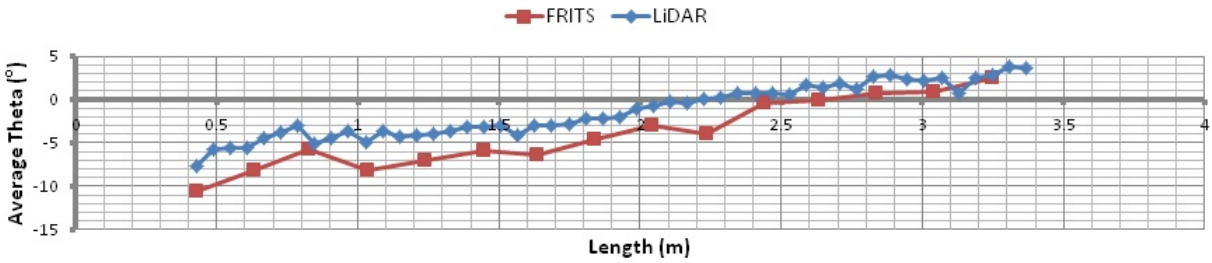

Figure 25: Angle theta - batten 1 comparison plot

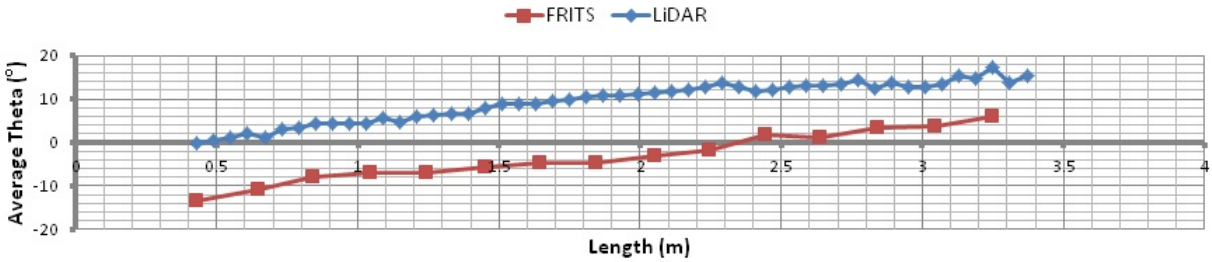

Figure 26: Angle theta - batten 2 comparison plot

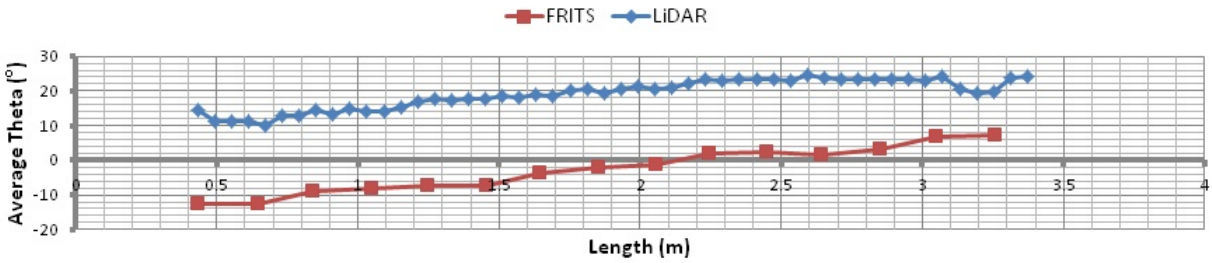

Figure 27: Angle theta - batten 3 comparison plot

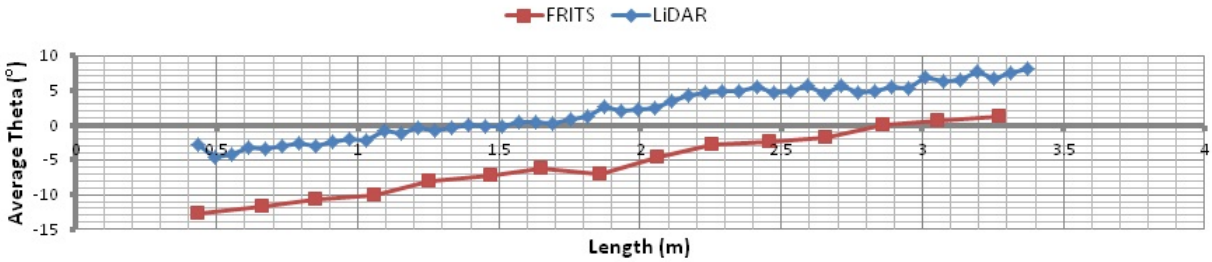

Figure 28: Angle theta - batten 4 comparison plot

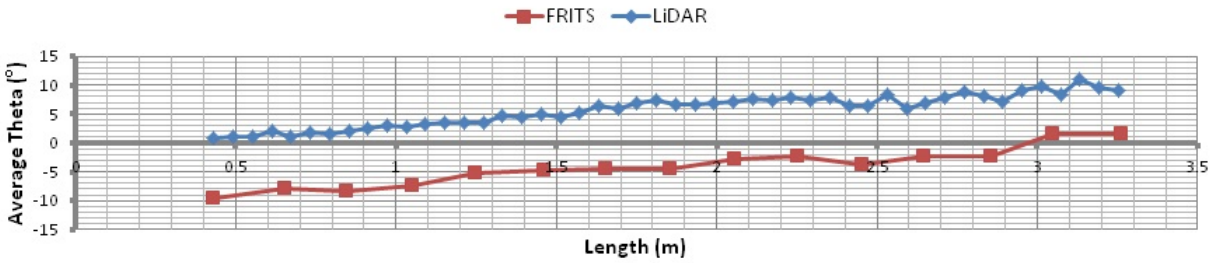

Figure 29: Angle theta - batten 5 comparison plot

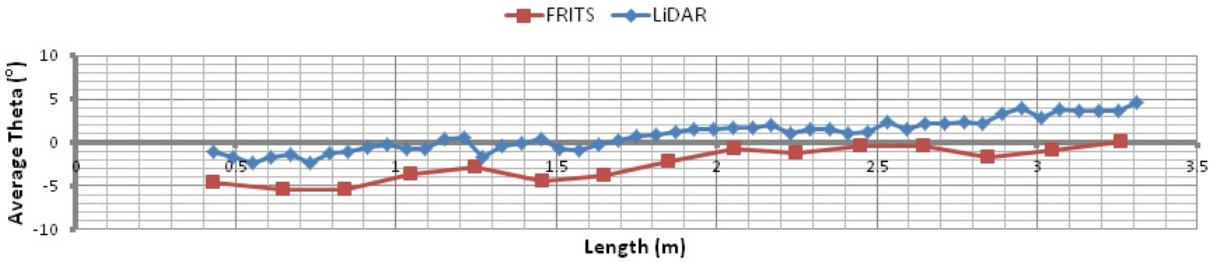

Figure 30: Angle theta - batten 6 comparison plot

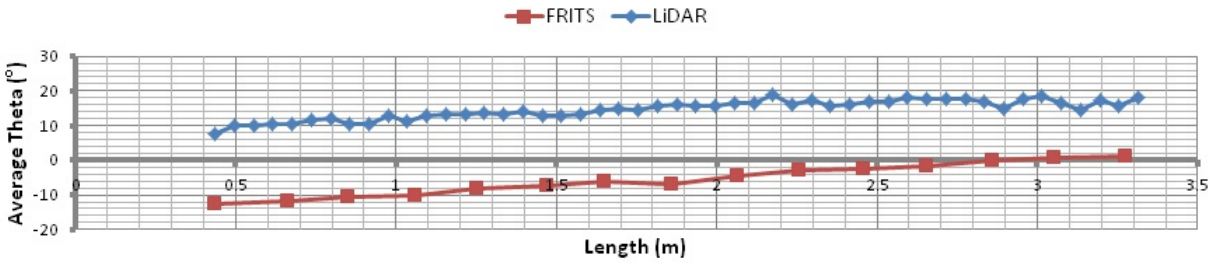

Figure 31: Angle theta - batten 7 comparison plot

These plots show the extent to which a timber batten surface can change along its length.

Note in the above plots that while the overall trend of θ_{ave} measurements is broadly matched by both methods, the absolute values of θ_{ave} measured by each method are different. LiDAR measurements consistently register larger values of θ_{ave} than FRITS. This is a consequence of how each method establishes a datum by which to takes its respective orthogonal measurements of batten surface distortion. This point will be discussed in detail within **section 7.2.1**

6.2.2 Change in Average Theta

Table 1 compares change in θ_{ave} ($d\theta_{ave}$) from both measurement methods for each batten 1-7.

Batten	**1**	**2**	**3**	**4**	**5**	**6**	**7**
$d\theta_{ave}^{FRITS}(^\circ/m)$	4.2	6.2	7.3	5.1	3.5	1.9	5.1
$d\theta_{ave}^{LiDAR}(^\circ/m)$	3.2	5.0	4.3	4.1	3.1	2.0	2.8
$\frac{d\theta_{ave}^{LiDAR} - d\theta_{ave}^{FRITS}}{d\theta_{ave}^{FRITS}}$	-0.24	-0.19	-0.41	-0.20	-0.11	0.05	-0.45

Table 1: Change in θ_{ave} - both methods

Standardising the changes in θ_{ave} measured by each method using the equation:

$$\frac{d\theta_{ave}^{LiDAR} - d\theta_{ave}^{FRITS}}{d\theta_{ave}^{FRITS}} \tag{23}$$

shows the results from the LiDAR method to be a good match overall with the FRITS standard. Measured values of $d\theta_{ave}$ for LiDAR differed from those

of the FRITS frame by a mean value of $-0.22^{\circ}/m$ with a standard deviation, $\sigma = 0.17^{\circ}/m$. A discussion of these results is presented in **section 7.2.1**.

6.3 Twist Measurements

Using the convention introduced in **section 6.1** a single of value of twist was extracted from each of the seven battens by means of both the FRITS and LiDAR scanning methods. The results are summarised in Table 2 below.

Batten	**1**	**2**	**3**	**4**	**5**	**6**	**7**
$Twist^{FRITS}(\%)$	0.0	3.1	2.9	-4.2	-5.0	0.0	-3.0
$Twist^{LiDAR}(\%)$	0.1	2.1	4.5	-1.0	-1.1	0.2	-3.0
$\frac{Twist^{LiDAR} - Twist^{FRITS}}{Twist^{FRITS}}$	/	-0.32	+0.55	-0.76	-0.78	/	0.00

Table 2: Twist - both methods

Measured values of $Twist$ for LiDAR differed from those of the FRITS frame by a mean value of -0.26% with a standard deviation, $\sigma = 0.56\%$. A discussion of these results is given in **section 7.2.2**.

6.4 Bow Measurements

Applying the measurement conventions described in **section 6.1**, a value of bow is calculated for each batten. The results are given in Table 3 below.

Batten	**1**	**2**	**3**	**4**	**5**	**6**	**7**
$Bow^{FRITS}(mm/2m)$	10.0	16.0	17.0	13.0	7.0	6.0	11.0
$Bow^{LiDAR}(mm/2m)$	9.6	19.6	17.6	13.1	10.0	7.0	8.9
$\frac{Bow^{LiDAR} - Bow^{FRITS}}{Bow^{FRITS}}$	-0.04	+0.23	+0.04	+0.01	+0.43	+0.57	-0.19

Table 3: Bow - both methods

Measured values of *Bow* for LiDAR differed from those of the FRITS frame by a mean value of $0.09mm/2m$ with a standard deviation, $\sigma = 0.20mm/2m$. A discussion of the above results is presented in **section 7.2.3**.

7 Comparative Analysis

7.1 Practical Aspects of Feature Measurement Experiments

Here, a comparative overview of some of the practical aspects of both measurement techniques is presented.

7.1.1 FRITS Experiments

The FRITS frame has the advantage of being a proven, established measurement technique. Set-up time of the apparatus itself is relatively minimal as the equipment is a stationary unit; and after a brief introduction, its use is largely straightforward. Measurements from both lasers can be input into a spread sheet immediately they have been taken using a Bluetooth connection between both lasers and a laptop. Given the repetitive and formatted nature of the scanning procedure it is possible to build up output calculations of distortion features while the scan is taking place, giving a finalised data set upon completion of the scan. This requires each batten to be scanned in the same way.

Scan time for each batten was around six to eight minutes. This included ensuring each batten was positioned firmly in place within the frame, carrying out test runs to ensure the vertical laser was on target along the length of the timber, as well as dealing with the inevitable glitches and interrupted signals incurred while using Bluetooth. This timescale only applies to the scanning of one surface per batten.

The size and bulk of the frame apparatus itself limits where and when the measurements can be carried out. The frame is a static piece of equipment and as such must always be worked around. Further, the manual nature of positioning the FRITS frame lasers incurs inaccuracies in establishing exactly where each laser measurement is positioned on the batten surface. The method assumes that the edge of the batten runs parallel to the direction along which the laser travels. This may be a suitable assumption for battens presenting little deviation from the central axis. However, this can become less justifiable as batten deformation increases.

7.1.2 LiDAR Experiments

The technical requirements for using a LiDAR scanner are somewhat greater than those of the FRITS frame. A trained technician is needed for both the set-up of the apparatus, as well as the post-scan editing required. Once set-up correctly, scan time for the chosen resolution was less than two minutes. If multiple scans of a batten are to be taken, the method only requires access to all sides of the batten. With this accounted for, resetting for another scan takes very little time. While markedly quicker to scan than the FRITS frame, LiDAR scanning does require a certain amount of post-processing of the point cloud data to eliminate unnecessary points. Additional manipulation is needed if multiple scans are to be combined.

Unlike the FRITS frame, LiDAR scanning can be carried out wherever there is room to comfortably manoeuvre the batten and the LiDAR unit. Weather

permitting, and with adequate power supply, it can also be performed outside, freeing it from the static constraints of the Freiburg method. Of particular note, LiDAR scanning does not require the often cumbersome and potentially costly transport of timber battens to the scan site. Rather, the relatively portable scanning equipment and battery supply can be taken to where they are needed, freeing up the measurement process and allowing a more flexible, adaptive approach to distortion measurement.

With the LiDAR method, however, measurements of distortion cannot be extracted directly and automatically from the raw data as in the FRITS method. Once the point cloud has been finalised, further information must be extracted from the data before distortion measurements can be taken. A datum from which distortion can be measured must be established first. With the FRITS frame scans, this datum is set automatically by the frame itself and remains constant for each experiment. However, each time a scan is carried out using LiDAR, the datum changes with the position of the scanner and the batten being measured. Calculating a reference surface from which deviations can be measured is a necessary first step in the new LiDAR method, and is unique for each scan (See **section 4.3** for a full explanation of the distortion code).

This additional analysis is a consequence of the substantially greater amount of input data gained from the LiDAR method as compared to the FRITS frame. The FRITS frame experiments took sixty measurements of each batten surface, whereas the point cloud used to describe each batten with the

LiDAR scanner consisted of around thirty-thousand points. Managing these larger figures and extracting meaningful measurements from them will therefore undoubtedly be subject to greater computational requirements.

However, the LiDAR scan does provide a much more comprehensive description of each unique batten surface: in stark contrast to the pointwise, interpolative measurements of the FRITS frame. Further, set-up and scan times for the LiDAR are considerably shorter and less tedious than those of the FRITS. Use of the FRITS frame requires positioning the batten within the frame such that a suitable number of points can be measured; the starting position for each scan length and the distances between them must be measured by hand, and a test run for each new scan length must be carried out to ensure the laser remains comfortably on the batten surface throughout. All of which generates an unavoidably lengthy scanning procedure.

In contrast, positioning of the batten for LiDAR scanning requires only that the scanner receives an uninterrupted view of the batten surface and that the batten remains stationary. No manual measurements need be taken of the batten during LiDAR scanning as these can be extracted from the point cloud data as necessary. Combined, these features allow for a greater number of battens to be scanned in a much shorter period of time compared to the FRITS frame. From a practical standpoint LiDAR scanning provides a quicker, more efficient solution to feature measurement.

7.1.3 Measurement Errors

The FRITS frame apparatus utilised two Leica DISTO lasers with a certified accuracy of ±2mm. For the LiDAR experiments a *FARO Photon 20/120 Laser Scanner* was used, also with a certified accuracy of ±2mm, as per the manufacturer's literature. In discussing the accuracy of laser scanning technologies, the range over which measurements are taken is important. Given the dimensions of the FRITS frame, vertical measurements of displacement were taken from around one meter from the surface of the batten. With the LiDAR set-up used, the scanner was similarly placed around one to two meters from the batten for each experiment. In this regard, the FRITS frame apparatus does ensure consistent, standardised measurements, while the movable nature of LiDAR opens itself up to discrepancies in the range over which it scans. However, the portable nature of the LiDAR is one of the things that recommends it over the static FRITS approach.

Further, the FRITS frame is subjected to a noticeable degree of vibration as the vertical laser moves along its track. Quantifying the impact of this movement on final accuracy is difficult. However, it is not inconceivable that a markedly distorted batten - say, for example, a batten presenting a significant degree of bow - could be disturbed from its resting position on the frame as the laser moves down the track. Any accidental movement of the batten during scanning could understandably produce inaccurate results. The issue of vibration is not a problem met with by the LiDAR scanner. Provided the scanner is positioned on a solid, stable footing, the equipment presents no noticeable degree of vibration.

Output from the FRITS frame lasers was given to the nearest 1mm, whereas LiDAR output was to the nearest one-hundredth of a millimetre. To ease comparison and to avoid spuriously 'precise' results, all final distortion feature measurements were given to one decimal place for both methods. This corresponded to batten measurements for bow and twist being taken to the nearest millimetre. For measurements of angle theta, the relevant batten measurements used in the calculations were also rounded to the nearest millimetre. Measurements were restricted in this way to allow easy comparison with the FRITS frame measurements, whose limits of accuracy only extended to the level of a millimetre. Further, specifications for distortion limits provided in the standards are only given to the nearest millimetre [**BS EN 14081-1, 2005**].

While the LiDAR produces measurements to a finer degree of detail than the FRITS, the lower specification of the FRITS equipment in addition to the accuracy prescribed in the standards mean that a comparison between the two methods was restricted to the FRITS frame's lesser measurement length scale. This being said, some insight was gained by the finer level detail of the LiDAR. For instance, two battens (battens 1 and 6) in the sample presented with 0.0% twist when measured by FRITS. Given that the battens were selected due to their failing of visual inspection, it seems unlikely that any of the battens did not present with some degree of twist. More likely rather is that the lower accuracy of the FRITS frame did not register enough of a discrepancy between vertical measurements at the millimetre scale to

generate a value of twist. However, with the LiDAR scanner a small degree of twist was registered in both battens. This potentially suggests that both its increased point density and measurement accuracy allows the LiDAR to recognise subtle features of batten shape not currently afforded by the FRITS.

7.2 Distortion Measurements

7.2.1 Change in Surface Inclination

Measurements of change in surface inclination as achieved by the LiDAR method compared well against those measured by the FRITS frame standard. However, with the exception of a small portion of batten 1, LiDAR measurements of θ_{ave} were larger than those of FRITS to a greater or lesser degree. This difference in magnitude is a result of the nature by which each method generates its respective datums, relative to the batten surface.

In the case of the FRITS frame the process is consistent and automatic for each scan. Vertical measurements are taken from the laser affixed to the upper supports of the frame structure. Each batten is lain on the lower frame supports, which run parallel to those above, while ensuring that three points of support are maintained. As such, the surface on which each batten sits is in plane with that from which measurements are taken. Thus, if a batten presents with only relatively minor distortion out of plane from the supports, then relatively smaller values of θ_{ave} will be recorded. With reference to the results presented in **sections 6.2.1-2**, batten 6, for instance,

shows a batten largely in plane with the FRITS structure, with a low value of $d\theta_{ave} = 1.9°/m$. It is interesting to note that with this low value of $d\theta_{ave}$, batten 6 recorded a twist value of 0%. Conversely, batten 3 recorded a larger value of $d\theta_{ave} = 7.3°/m$, and a subsequently larger value of twist = 2.9%.

With the LiDAR method presented here, however, the position of the datum is much more arbitrary, tailored each time to the batten under consideration. The reference surface from which deviations are measured is described by relatively few points along the short and long edges of the batten. Indeed, both the x^R and y^R axes were defined by just three points in total: one shared point at the approximate corner of the 'top' end of the batten which served as the reference origin, and one point along the adjacent short and long edges to define the x^R and y^R axes respectively.

This point-wise approach stands in contrast to the FRITS method. In this instance, the extent to which the batten has distorted will determine how it rests on the support surface; however, that surface will always remain in plane with the surface from which measurements are taken. On the other hand, the LiDAR is much more susceptible to generating a reference surface that is markedly more out of plane with the batten surface itself. This seems to be the case in the measurements of θ_{ave}, where the magnitudes of angle θ_{ave} were consistently larger for LiDAR than with FRITS. Figure 32 below compares how a difference in orientation between FRITS and LiDAR measurements can lead to a difference in magnitude for avalue of θ_{ave} at an arbitrary point along the batten length.

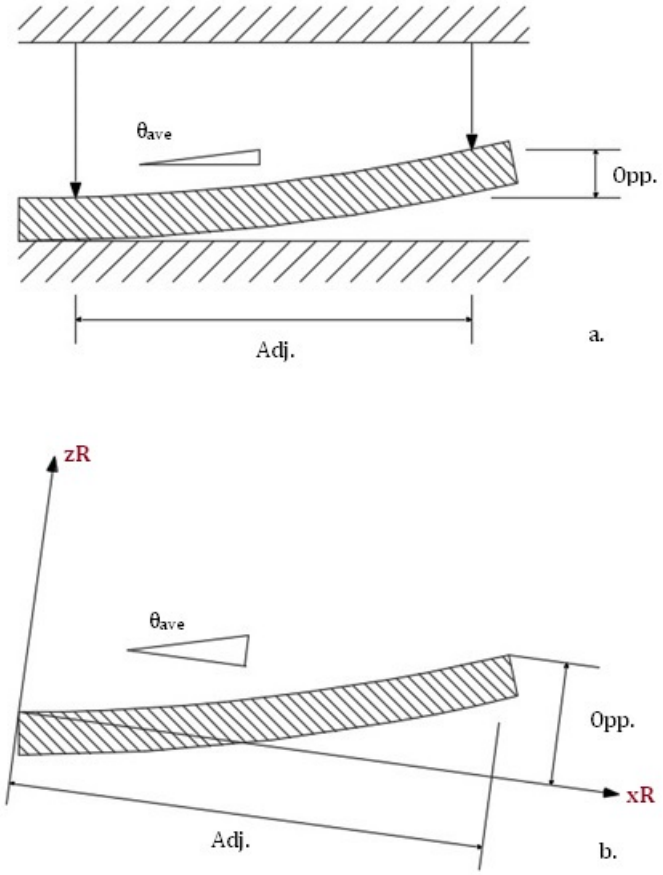

Figure 32: a. FRITS measurement of angle θ_{ave}
b. LiDAR measurement of angle θ_{ave}

Note, however, that while the LiDAR method registered larger values of θ_{ave} than the FRITS scans, the overall *change* in θ_{ave} ($d\theta_{ave}$) was in fact slightly less for each batten. This point is developed in detail in **section 7.2.4**.

As was to be expected with using such a large data set, the LiDAR scans generated much more variable measurements of surface inclination, as the plots of average theta in Figures 25-31 attest. Still, even with the far larger amount of measurement, a linear trend line applied to the measurements of angle θ_{ave} show relatively smooth curves, comparing well with the much more limited measurements produced by the FRITS scans. This smoothness could be improved further by increasing the resolution of the reference grid to generate an even greater number of measurements. It must be noted, however, that this increase would naturally entail a greater computational burden. This point of reference grid resolution is developed further in **section 8.2**.

Across all seven battens, the LiDAR method was able to accurately and reliably reproduce $d\theta_{ave}$ results gained from the FRITS standard.

7.2.2 Twist

Overall, measurements of twist gained from the new LiDAR approach compared well with those achieved by FRITS. Unlike measurements of $d\theta_{ave}$, where trends over the length of the batten were considered, single values of twist were extracted at a specific length from each batten end. In this way, discrepancies between measurement datums of both methods discussed above were somewhat more influential in determining degrees of twist than was apparent in measurements of surface inclination.

Prescriptions for measuring twist in accordance with European Standards

require one long side of the batten to be laid on a flat surface while the height of the opposite long side is recorded at a length of two metres from the batten end. This height (y) is divided by the batten width to give a measure of twist, with the final value being expressed as a percentage.

In the FRITS frame experiments, each batten was rested on the frame supports along its 'Right' side, as per the convention described in **section 6.1**. Measurements of height were then taken from the opposing 'Left' edge. In this way, the 'Right' side of each batten was prescribed as being the lower side, with height measurements (y) recorded relative to it. With the LiDAR method, however, the reference axes were positioned such that y^R axis was aligned along the 'Left' long side of the batten. By this convention, the 'Left' long side of each was prescribed as the lower side. This difference in orientation had to be considered when extracting values of 'y' from point cloud data in order to match the convention established by FRITS. This ensured that the LiDAR data matched the FRITS data in terms of its sign convention. However, the magnitude of twist measurements differed to varying degrees across the sample battens.

These differences in magnitude of twist as measured by LiDAR in comparison to FRITS were largely a result of the arbitrary placement of the reference surface discussed above. Three out of the seven battens scanned measured a value of twist less that measured by FRITS, with a fourth giving batten matching the value of twist (rounded to one decimal place). This corresponds strongly with the trend observed with measurements of change in surface in-

clination whereby the LiDAR consistently recorded lower values than the FRITS frame.

In a similar way to measurements of the change in surface inclination, measurements of twist essentially record a change in height across the batten surface- not lengthwise, as with surface inclination, but rather laterally across the batten width. In this way, the height of one side of the batten (y) is measured by it's relative position to the height of the other side which is assumed to be on a flat, level surface. Where the reference axes are not fully aligned with the plane of the batten surface, values of orthogonal deviation used to calculate height 'y' may incur additional offsets making a faithful comparison with the more standardised FRITS method more challenging.

7.2.3 Bow

Many of the issues raised in the comparisons between measurements of both surface inclination and twist obtain for bow. Overall, measurements of bow using LiDAR matched strongly with those gained from FRITS. As discussed above, the LiDAR measurements presented differing magnitudes of bow compared to those measured by FRITS; however, with bow measurements, these differences were relatively small across the sample set.

7.2.4 Distortion Measurements Summary

Concerning the magnitudes of distortion values, in five of the seven battens scanned, the LiDAR method recorded a larger value of bow than FRITS. It is interesting to note that of the four feature measurement types considered

here, surface inclination (θ_{ave}) and bow generally recorded larger values with the LiDAR method than the FRITS; while both change in surface inclination ($d\theta_{ave}$) and twist tended to record lower values for the LiDAR method. These trends may provide insight into how the reference axis placement performs and help guide efforts to more a standardised, reliable approach in the future. For now, these discussions will help inform any comparisons between FRITS and LiDAR

Those feature measurements that recorded larger values with the LiDAR model (θ_{ave} and bow) considered only single measurements at a specific point on the batten surface. In the case of θ_{ave} this was the angle of the surface at prescribed intervals. With bow it was the maximum deviation from the longitudinal axis along a two metre length of one edge of the batten. These measurements did not consider any relative change in the batten surface, nor the relationship of one portion of the batten with another. Rather, they concerned only direct measurements of the batten relative to the reference surface. Surface inclination with the LiDAR method was a measure of the slope of the batten surface relative to the reference surface. Similarly, in measuring deviations along a two meter-length of one long edge and selecting the maximum value to calculate bow, the final result recorded was directly dependent on the spatial relationship of the batten and reference surface.

Conversely, measurements of $d\theta_{ave}$ and twist recorded relationships of the batten relative to itself. Change in surface inclination considered how the slope of the batten altered from one end to the other along the longitudinal

axis. Twist considered the projecting height of one side of the batten relative to the other side. In this way, the relationship between the batten and it's measurement datum was of little consequence. Only changes across the batten were measured.

As such, in assessing the discrepancies brought about by the arbitrary placement of the reference axes, the issue of axis positioning is more pertinent to measures of θ_{ave} and bow. Additionally, from the definitions established in the European standards, measurement of spring would also be dependent on the placement of the reference axis. In these instances, a formalised, universal placement system would be required to provide more reliable comparisons between LiDAR and FRITS. With measurements of change in surface inclination and twist (and cup as per European standards), however, reference axis placement and orientation becomes less important. In this way, a stronger comparison can be made between results from the new LiDAR method and the FRITS frame.

Notwithstanding some of the issues raised regarding the comparison between FRITS and LiDAR, it is interesting to note that both methods recorded an apparent correlation between measured values of change in surface inclination, twist and bow. From the relatively small selection of batten samples used in this thesis, a higher measurement of change in surface inclination tended to correspond to greater values of both twist and bow. Both FRITS and LiDAR recorded the highest values of each of these measurements in battens two and three. For lower values of $d\theta_{ave}$, the comparison breaks

down somewhat with LiDAR measurements of twist. Among the batten samples, FRITS recorded a lowest value of $d\theta_{ave}$ in batten 6 ($1.9°/m$). Correspondingly, FRITS measured the lowest values of twist and bow in batten 6 (0% and 6mm/2m, respectively). For twist measurements, this was not fully captured with the LiDAR method. However, the trend was replicated much more reliably with measurements of bow, where again one of the lowest measurements were recorded in batten 6 (9.4mm/2m).

7.3 Weighted Averaging Method - Comparison with Gaussian Weighting Function

In **Section 4.3.7** a method was introduced by which a measure of orthogonal deviation could be estimated for each point on the reference grid by averaging the orthogonal deviations of the surrounding LiDAR points. However, the weighted averaging method used, shown in Equation 16, is only one possible method and others exist. Given that the weighting method is used to establish final orthogonal deviations across the reference grid points, it's influence on the measurements extracted from the LiDAR model is clear. For this reason, an investigation was carried out to assess what impact was made on final distortion measurements by using an alternative weighted averaging fucntion.

Alexa et al. [**2003**] describe a typical Gaussian weight function that can be applied to averaging procedures with point data sets. The weight function is as follows:

$$W_i = e^{\frac{\Delta_i^2}{H^2}} \tag{24}$$

Where:

Δ_i = geodesic distance of neighbourhood point to reference grid point

H = parameter representing the geodesic distances between points within the neighbourhood

Levin [**2004**] specifies the 'H' parameter as the average distance between data points. Accordingly, the mean spacing between points within each LiDAR scan was used for the value of 'H'.

As can be seen, the influence a point has in determining the final orthogonal deviation falls off exponentially the further the point is from the reference grid point. Thus, the averaged measurement tends to greatly favour those points closer to the measurement point.

The average orthogonal deviation of each reference grid point is calculated by multiplying the orthogonal deviation of each neighbourhood point by the above weighting function and summing. This is shown in Equation 25.

$$z_{ave} = \sum_{i=1}^{n} W_i z_i^R \tag{25}$$

Where:

z_i^R = orthogonal deviations of neighbourhood points

7.3.1 Change in Surface Inclination with Gaussian Weighting Function

Below is a reproduction of the average theta plots given in **section 6.2.1** with the addition of average theta measurements as calculated using average orthogonal deviations determined by a Gaussian weighting function. These are plotted in green. The methods by which average theta values were extracted from the LiDAR point cloud sets remain the same as discussed previously in **section 4.3**.

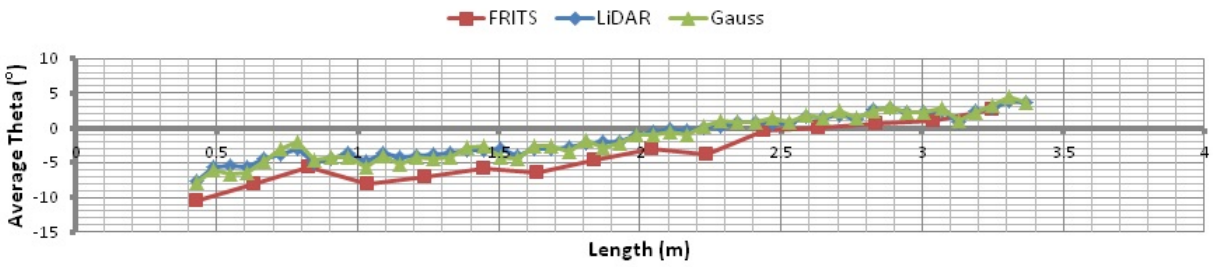

Figure 33: Angle theta - batten 1 comparison plot with weighted Gauss function

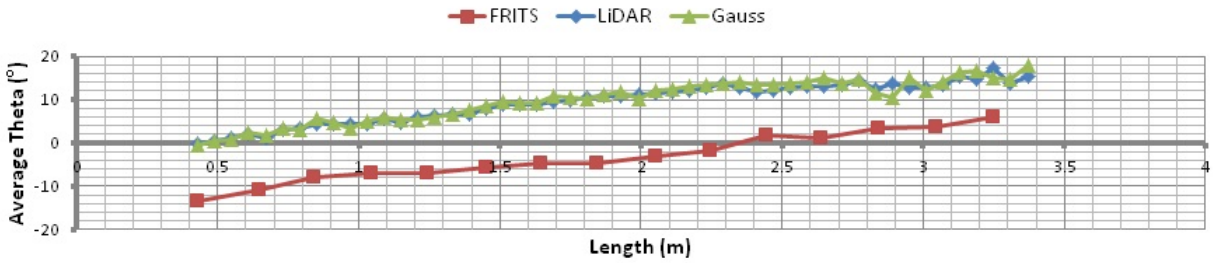

Figure 34: Angle theta - batten 2 comparison plot with weighted Gauss function

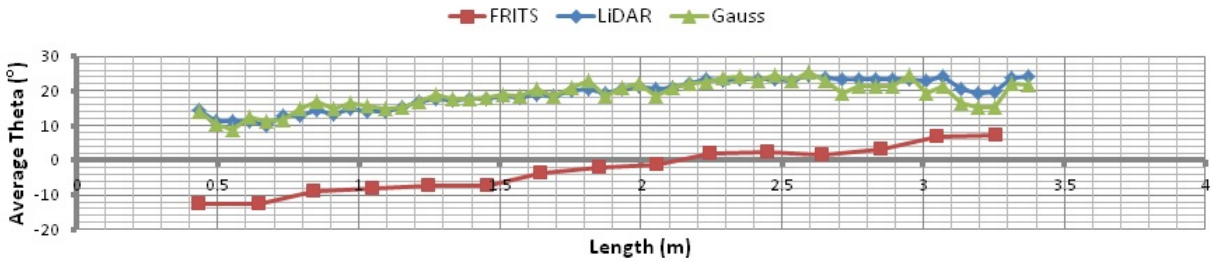

Figure 35: Angle theta - batten 3 comparison plot with weighted Gauss function

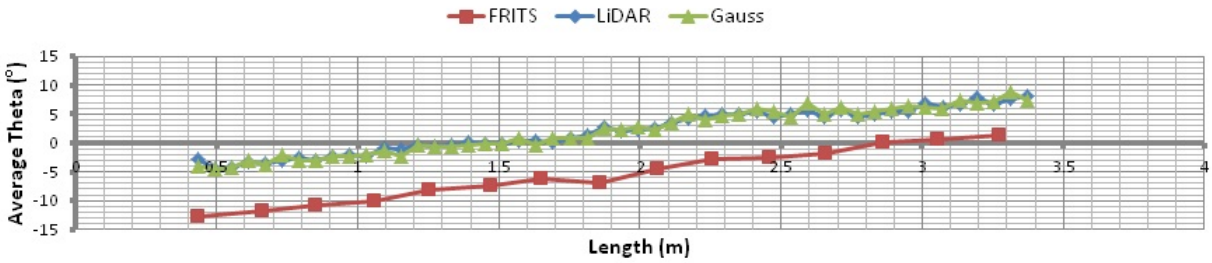

Figure 36: Angle theta - batten 4 comparison plot with weighted Gauss function

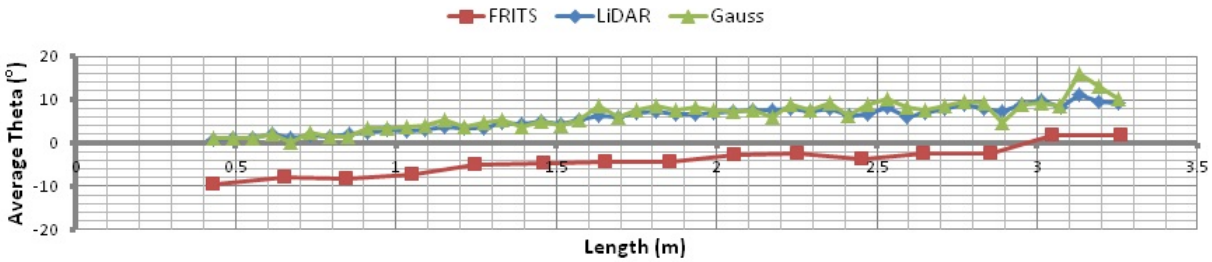

Figure 37: Angle theta - batten 5 comparison plot with weighted Gauss function

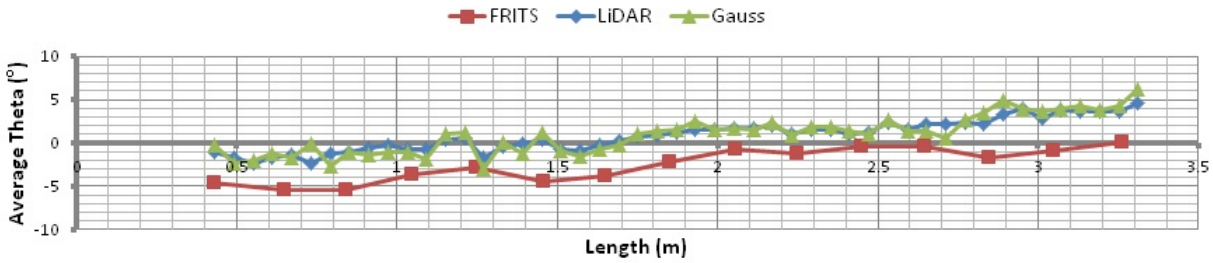

Figure 38: Angle theta - batten 6 comparison plot with weighted Gauss function

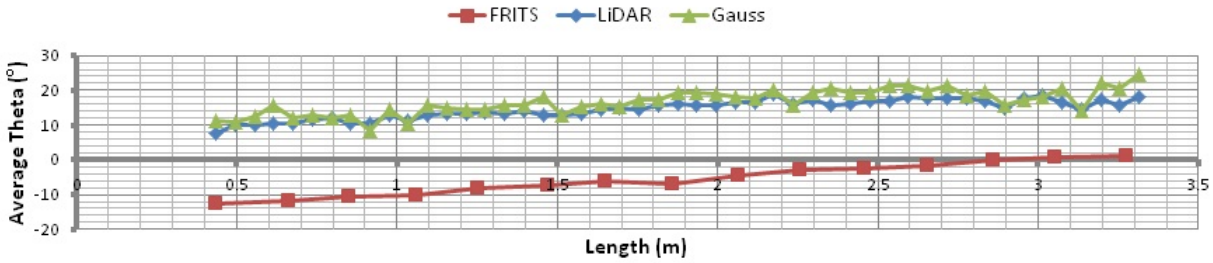

Figure 39: Angle theta - batten 7 comparison plot with weighted Gauss function

From the above plots we can see that the effect of the Gaussian weighting function would appear minimal. Overall, the values for θ_{ave} using the Gaussian weight function match closely (but not exactly) to those calculated using the linear weight function. In comparing the values of θ_{ave} as measured using each weight function, the largest discrepancies between the two tended to be

within those measurements taken at the ends of the battens. These areas at the ends of each batten tended to be where the fit of the reference grid to the projected reference surface was somewhat less precise and the reference grid rows did not align exactly with the often rather scattered arrangement of the reference surface points. As such, the neighbourhood searches along these rows struggled to produce a cogent measurement of orthogonal deviation. These discrepancies seem to have been further affected by the change of weight function.

As before, a measure of the change in surface inclination was calculated with the Gaussian weight function. These results are summarised in Table 4 below, along with the original values obtained from the FRITS and LiDAR methods.

Batten	**1**	**2**	**3**	**4**	**5**	**6**	**7**
$d\theta_{ave}^{FRITS}(^\circ/m)$	4.2	6.2	7.3	5.1	3.5	1.9	5.1
$d\theta_{ave}^{LiDAR}(^\circ/m)$	3.2	5.0	4.3	4.1	3.1	2.0	2.8
$d\theta_{ave}^{LiDAR}(^\circ/m)$ **[Gauss]**	2.8	3.3	3.2	4.4	3.5	2.2	3.3
$\frac{d\theta_{ave}^{LiDAR} - d\theta_{ave}^{FRITS}}{d\theta_{ave}^{FRITS}}$ **[Gauss]**	-0.33	-0.47	-0.56	-0.14	0.00	0.16	-0.35

Table 4: Change in θ_{ave} - comparison with Gaussian weight function

Table 4 above helps clarify to what extent a Gaussian weighted average impacts the measured results of $d\theta_{ave}$. From these values (and indeed from the average theta plots), the substitution of a linear weighted average for a Gaussian function does not dramatically alter the results or the broad conclusions made regarding the method described in this thesis. Nevertheless, altering the weighted averaging method used has generated slightly different results from the LiDAR model. These results are discussed in **section 7.3.4**.

7.3.2 Twist Measurements with Gaussian Weighting Function

Twist measurements were repeated as described previously. Table 5 presents a summary of the original twist measurements from FRITS and LiDAR, with the inclusion of equivalent measurements using the Gauss weight function.

Batten	**1**	**2**	**3**	**4**	**5**	**6**	**7**
$Twist^{FRITS}(\%)$	0.0	3.1	2.9	-4.2	-5.0	0.0	-3.0
$Twist^{LiDAR}(\%)$	0.1	2.1	4.5	-1.0	-1.1	0.2	-3.0
$Twist^{LiDAR}(\%))$ **[Gauss]**	0.1	2.4	4.6	-1.1	-1.1	0.2	-3.8
$\frac{Twist^{LiDAR} - Twist^{FRITS}}{Twist^{FRITS}}$ **[Gauss]**	/	-0.23	0.59	-0.74	-0.78	/	0.27

Table 5: Twist - comparison with Gaussian weight function

Reviewing Table 5 we can see that, as with measurements of $d\theta_{ave}$, the inclusion of a Gaussian weight function had a small impact on the final values of twist. The revised model tended to generate somewhat larger values of

twist with the Gaussian weighting function than the original linear approach, but not markedly so.

7.3.3 Bow Measurements with Gaussian Weighting Function

Bow measurements were generated as before with the inclusion of the Gaussian weighting function. The results are given in Table 6 below.

Batten	**1**	**2**	**3**	**4**	**5**	**6**	**7**
$Bow^{FRITS}(mm/2m)$	10.0	16.0	17.0	13.0	7.0	6.0	11.0
$Bow^{LiDAR}(mm/2m)$	9.6	19.6	17.6	13.1	10.0	7.0	8.9
$Bow^{LiDAR}(mm/2m)$ **[Gauss]**	10.4	21.6	16.1	14.7	10.1	8.4	15.5
$\frac{Bow^{LiDAR} - Bow^{FRITS}}{Bow^{FRITS}}$ **[Gauss]**	0.04	0.35	-0.05	0.13	0.44	0.40	0.41

Table 6: Bow - comparison with Gaussian weight function

Table 6 shows that overall, with the inclusion of the Gauss function, measurements of bow calculated by the LiDAR model tended to be slightly larger than those from the previous iteration. As with other feature measures, the difference appeared minimal.

7.3.4 Summary

This section has provided a useful insight into some of the underlying features of the model presented in this thesis. Questioning some of the choices made in constructing the original measurement model and assessing the impact of alternative approaches aids in the overall evaluation of the model's efficacy.

Given the focus of this thesis is to compare the LiDAR model with the established standard of the FRITS method, reviewing Tables 4-6 we can see that the inclusion of the Gauss function tended to broaden the gap between FRITS measurements and LiDAR measurements.

In assessing the impact of using a Gaussian weighting function to average orthogonal deviations within each neighbourhood, the size of the neighbourhoods themselves does not appear to be of great significance. Increasing neighbourhood size 'k' from ten (the standard used throughout this thesis) to fifty does not have any appreciable impact on the final distortion measurements gained. Rather, the issue may be a question of scan resolution. In their investigations into rendering point cloud samples, Alexa et al. discuss the use of a Gaussian weighting function in the context of using dense and often highly complex point clouds. These are far in advance of the medium-range resolution scans used in this thesis. It may be that to achieve the full benefits of an alternative weighting function, much denser, more detailed scans would have to be carried out than were used in the experiments here.

In comparing the two averaging methods, while the differences in magni-

tude may appear numerically small, there is a potential that these differences could impact on the final grading of a batten. For example, in the measurement of bow in batten 2, both the FRITS and original LiDAR methods give a value of bow less than 20mm/2m. In accordance with BS EN 14081-1, this would meet the criteria for strength class C18 [**BS EN 14081-1, 2005**]. However, with the inclusion of the Gaussian weight function, the updated LiDAR model gives a value of bow of 21.6mm/2m, i.e. slightly above the threshold of maximum bow permissible for class C18. It is worth noting, though, that the moisture content at which these battens were assessed was lower than that at which distortion is typically measured. Considering this low moisture content, a bow measurement of 21.6/2m could be considered acceptable. It is interesting to note that across all three measurement methods (the FRITS, the LiDAR and the updated LiDAR) and across all three feature measurements taken, batten 2 tended to be present one of the largest degrees of distortion in the sample set used. Note also that the discrepancies between FRITS measurement values and LiDAR measurement values for batten 2 tended to be among the largest for measurements of $d\theta_{ave}$ and bow among the seven battens scanned.

It would appear then that in having greater disparities between orthogonal deviations of reference surface point - or in other words, a greater degree of distortion across the batten - the impact of the weighted averaging of those deviations seems to be more apparent. Where there is little distortion to measure, in batten 6 for example, the differences between feature measurements with a linear weighted averaging and a Gaussian equivalent seem to diminish.

With consideration of the above points, a thorough assessment of alternative weighted averaging schemes would benefit from using higher resolution scans than those used here. While far in excess of anything that can be achieved with the FRITS, the LiDAR scans used for this project limited themselves to a medium resolution level - relatively sparse in comparison to the higher resolutions available. Further, the small sample size used here seemed to indicate that the greatest impact of a change in weighted averaging appeared to be present in those battens showing the greatest degree of distortion. Accordingly, future experiments would benefit from focusing on battens showing sizeable levels of distortion.

8 Discussion

Beyond the practical and quantitative comparisons between FRITS and LiDAR scanning, these investigations have generated a number of observations, conclusions and recommendations regarding the broader issue of feature measurement of timber battens and the existing measurement standards by which battens are judged. Further, the experimentation with LiDAR scanning has suggested new ways in which the approach could be exploited and developed further in timber research, with particular reference to feature measurement.

8.1 Existing Standards

It was noted in **section 1.3** that this research was in part motivated by the deficiencies within standards BS EN1310:1997. These investigations have highlighted some of these pre-existing issues and have given further credence, if any were required, to the need for re-evaluation. The work into creating a new feature measurement technique has generated specific recommendations as to how the existing standards could be added to and improved.

From a geometric standpoint, the existing standards may appear to be exhaustive: the four measures of deviation (bow, spring, cup and twist) seem to account for all the possible ways and directions in which a rectangular batten may deviate. However, the standards limit themselves to using maximum values of deviation along single measurement lengths. On the other hand, a measurement of the change in surface inclination ($d\theta_{ave}$), whereby a greater proportion of the batten surface is covered, in both lateral and

longitudinal directions, may be a worthwhile addition to the existing feature measurement approach.

A comparison of the measured values of $d\theta_{ave}$ and twist from LiDAR scanning shows while higher degrees of twist (approximately between 2-4% within the sample set used here) shows a strong correlation with a higher degree of $d\theta_{ave}$, the same does not appear to be true for low values of twist (approximately 0% rounded to 1 decimal place). For example, with reference to Table 7, we can see that batten 1 recorded a value of $d\theta_{ave} = 4.2°/m$ with the FRITS frame. However, using the same FRITS method, batten 1 recorded no twist (Note, a similar result was produced using the LiDAR method where a value of $d\theta_{ave} = 3.2°/m$, compared to a relatively low twist measurement of 0.1%).

Batten	**1**	**2**	**3**	**4**	**5**	**6**	**7**
$d\theta_{ave}^{FRITS}(°/m)$	4.2	6.2	7.3	5.1	3.5	0.2	5.1
$Twist^{FRITS}(\%)$	0.0	3.1	2.9	-4.2	-5.0	0.0	-3.0

Table 7: Comparison of $d\theta_{ave}$ and twist measurements- FRITS frame

It is clear then that the current approach of taking measurements along a single scan length does not necessarily provide a true indication of change in the surface inclination. Here, there is a potential that pertinent features of

the batten surface are not begin captured. Instead, measurements that track a wider surface area along the batten length, such as $d\theta_{ave}$, may provide a more representative insight into changes of batten surface morphology and could serve as an important addition to current standards.

Existing standards could be re-written then to adopt a more holistic approach to feature measurement. Standards could utilise measurements that consider the batten more holistically and cover a larger area of the batten surface, registering changes in deviation across the full length of the batten. With the introduction of LiDAR scanning technologies, this increase in measurement sampling could be handled in a timely, efficient and accurate way.

8.2 Outlook for the Use of LiDAR Scanning Within Timber Research

Experimentation with the LiDAR scanner revealed a number of new areas of potential interest from which future researches in feature measurement may benefit. These ideas exploit the practical nature of LiDAR scanning in order to further expand upon the existing FRITS frame approach.

With LiDAR scanning it would also be possible to scan the thinner, adjacent edges of the batten to gain detailed distortion measurements not currently possible using the FRITS. Spring, as defined in EN 1310:1997 could be measured easily using the same method described in this thesis, only with the batten turned 90° such that its thin edge is presented to the scanner. From

this, plots of how the batten edge deviated from an undeformed datum could be generated, giving a comprehensive measure of spring. Such detail would not be possible with the current FRITS method. A batten resting on its narrow edge within the frame presents a very limited area along which measurements could be taken. Using the FRITS equipment, such an approach allows for, at most, two scan lengths to be taken; in some cases only one is possible. This incurs a great deal of interpolation between measurement points and provides little insight into the actual morphology of the batten edge.

Similarly, profiles of the end surface could be generated and analysed using LiDAR. Not only could this aid in the measuring of cup, for example, they could also generate a comparison for how the batten profile changes from one end of the batten to the other. End profiles like these cannot currently be replicated using the current method as the FRITS is limited to only lengthwise scans.

In **section 7.2.1** the potential for expanding the resolution of the reference grid to give highly detailed measurements was touched upon. Measurements of the batten ends could provide a avenue for further expansion of the LiDAR method as an accessible, smaller-scale alternative to industrial-sized scanners. Currently, commercial laser scanners (such as the *WoodEye* Scanner) can provide accurate, highly-detailed measurements, not just of batten geometry but also of wood grain patterns. It is posited here that using a high resolution LiDAR scan of the batten end at close range could, for example,

allow analysis of the annual growth rings or accurate positioning of the pith. The problem would reduce down to an assessment of geometric information, much like the solution presented in this thesis. The challenge, however, would be in the successful management of significantly higher, more concentrated point cloud data points. Nevertheless, the LiDAR method aims to provide an accessible, practical comparative tool for timber analysis. Assessment of annual growth rings is another possible area for expansion.

A natural progression of the LiDAR method is the use of three-dimensional scans to describe the shape of the entire batten and not just one surface. With the FRITS frame, measurements can be taken of both surfaces of a batten and compared, the process is cumbersome and time consuming. To scan two surfaces of a batten with the FRITS effectively doubles the work load and proves an inefficient and often tedious process. However, multiple LiDAR scans can be carried out with relative ease providing there is enough room to manoeuvre around the batten. A minimum of two scans are required to achieve a full 360° scan of a timber batten. This can be carried out within five minutes on a medium scan resolution: far quicker and easier than the FRITS. The process would require additional manipulation of the point cloud data in order to map individual scans together to form a complete 3D model. This is a standard requirement for many who work with LiDAR scanning and such manipulation is easily provided for by the necessary software.

This research, and indeed the British Standards themselves, considered measurements along one surface only and assumed the batten to be a rigid body,

with the deviation of one surface being matched by the surface underneath. These may prove to be suitable assumptions in most cases; however, further investigation is recommended to verify this. Although FRITS scans of opposing surfaces have been carried out by colleagues, again the necessarily high interpolation required of the FRITS method may not be providing a full picture of how the surface alters. Adopting the LiDAR scanner would provide an efficient and more accurate alternative to this task.

9 Conclusion

For measurements of the change in surface inclination ($d\theta_{ave}$), the LiDAR method developed in this project consistently compared well with the results obtained by the standard FRITS approach. Comparing final outputs from the LiDAR with those of the FRITS, the LiDAR method differed from the standard FRITS frame measurements by a mean value of $-0.22^{\circ}/m$ ($\sigma = 0.17^{\circ}/m$). In six out of the seven battens scanned, the LiDAR method measured the change in surface inclination to be lower than that of the FRITS frame.

Similarly, for measurements of the degree of twist along the leftmost edge, the LiDAR method produced results comparable to those obtained by FRITS. The LiDAR measurements differed from the FRITS standard by a mean value of -0.26% ($\sigma = 0.56\%$). Using LiDAR the degree of twist was found to be higher than that found by FRITS in all but one of the seven battens.

In measuring bow, values extracted from LiDAR scans differed from those of the FRITS method by an average value of $0.09mm/2m$ ($\sigma = 0.2mm/2m$). In five out of the seven battens, the LiDAR method produced results for bow that were larger than that obtained by FRITS.

The ongoing need for reassessment of existing standards was also highlighted in this work. The investigations here have lead to the recommendation of an expansion of BS EN 1310:1997 to include a standardised measure of surface inclination (θ_{ave}) in its list of distortion features. Currently, fixation on 'rep-

resentative lengths' to measure batten distortion do not paint an accurate picture of batten morphology, nor are they broadly applicable to all battens. Rather, the inclusion of a distortion feature more representative of the surface as a whole would be a worthwhile addition to the feature measurement standards. The increase in surface measurements required of this approach, while cumbersome with the existing FRITS frame method, could be readily and efficiently met by utilising LiDAR scanning technologies.

*

This thesis has helped introduce the use of LiDAR scanning to the field of timber distortion measurement. It has served as a crucial proof of concept for a heretofore untapped resource in a fertile area of timber research. It is the hope of this work that the investigations detailed here have presented LiDAR scanning as a viable, reliable new approach to distortion feature measurement. Over reliance on a single measurement method will struggle to provide new insights or improvements in distortion feature analysis, and as such, the field may stagnate and fail to address the issues it currently faces. The work in this report has confirmed that LiDAR scanning can produce comparable results to the existing FRITS method, while being a far more efficient, more practical approach. The technique also allows for further development of the feature measurement process not currently capable with existing methods. As such, the groundwork has been laid for LiDAR scanning to become an approved and standard approach to measuring macroscopic deformations of timber battens.

10 References

Alexa, M., Behr, J., Cohen-Or, D., Fleishman, S., Levin, D. and Silva, C.T. (2003). Computing and Rendering Point Set Surface. *IEEE TRANSACTIONS ON VISUALIZATION AND COMPUTER GRAPHICS*. **9**, pp.3-15.

Almeida, G. and Hernández, R.E. (2006). Changes in physical properties of tropical and temperate hardwoods below and above the fibre saturation point. *Wood Science Technology*. **40**, pp.599-613.

Bergander, A. and Salmn, L. (2002). Cell wall properties and their effects on the mechanical properties of fibres. *Journal of Materials Science*. **37**, pp.151-156.

Brändström, J. (2001). Micro- and ultrastructural aspects of Norway spruce tracheids: a review. *IAWA Journal*. **22**, pp.333-353.

British Standards Institute (1997). BS EN 1310:1997. Round and sawn timber - Method of measurement of features. BSi.

British Standards Institute (2016). BS EN 14801-1. Timber structures Strength graded structural timber with rectangular cross section Part 1: General requirements. BSi.

Christensen, G.N. and Hergt H.F.A. (1969). Effect of previous history on kinetics of sorption by wood cell walls. *Journal of Polymer Science*. **7**,

pp.2427-2430.

Christensen, G.N. and Kelsey, K.E. (1959). The rate of sorption of water vapour by wood. *Holz Roh Werkst.* **17**, pp.178-188.

Curvescan [online]. (2016). Available from: http://microtec.eu/assets/products/curvescan/Microtec-Curvescan-Optiside-1.pdf. [**Accessed 21st August 2016**].

Du, S. and Yamamoto, F. (2007). An Overview of the Biology of Reaction Wood Formation. *Journal of Integrative Plant Biology.* **49**(2), pp.131-143.

Eitelberger, J. (2011). *A multiscale material description for wood below the fibre saturation point with particular emphasis on wood-water interactions.* PhD thesis, Vienna University of Technology.

Ekevad, M. (2005). Twist of wood studs: dependence on spiral grain gradient. *Journal of Wood Science.* **51**, pp.455461.

Engelund, E.T., Thygesen, L.G., Svensson, S and Hill, C.A.S. (2012). *A critical discussion of the physics of wood-water interactions.* In: COST Action FP0802, 2008-2012: Experimental and computational micro-characterization techniques in wood mechanics, 25 October 2012, Edinburgh.

Forestry Commission [online]. (2003). Available from: http://www.forestry.gov.uk/fr/infd-4xgjc8.

[**Accessed 4th January 2016**].

Fransden, H.L. (2007). *Selected constitutive model for simulating the hygromechanical response of wood*. PhD thesis, Aalborg University.

Goldeneye [online]. (2016). Available from: http://microtec.eu/en/catalogue/products/goldeneye300/. [**Accessed 21st August 2016**].

Grohmann, R., Aleon, D., Knaggs, G., Lagana, R. and Baso, C. (2010). COST Action E53 [online]. Available from: http://www.coste53.net/index.php?Activities:Publications:Distortion_of_Sawn_Timber
[**Accessed 2nd January 2016**].

Hill, C.A.S., Norton, A.J. and Newman, G. (2010). Water vapour soprtion properties of Sitka spruce determined using a dynamic vapour sorption apparatus. *Wood Science Technology*. **44**, pp.497-514.

Hill, C.A.S., Keating, B.A., Jaluladin, Z. and Mahrdt, E. (2012). A rheological description of the water vapour sorption kinetics behaviour of wood invoking a model using a canonical assembly of Kelvin-Voigt elements and a possible link with sorption hysteresis. *Holzforschung*. **66**, pp.35-47.

Holland, C. and Reynolds, T. (2005) Timber grading and scanning. *BRE Digest*. **492**.

Johansson, M. (2006). *Problem with distortion in timber Background and explanations*. In: COST Action E53 - International Workshop in Sopron, 9th November 2006, Sopron. pp. 100-125.

Johansson, M. and Ormarsson, S. (2009). Influence of growth stresses and material properties on distortion of sawn timber numerical investigation. *Annals of Forest Science*. **66**, pp.604-614.

Krabbenhft, K. (2003). *Moisture transport in wood: A study of physical mathematical models and their numerical implementation*. PhD thesis, Technical University of Denmark.

Lukacevic M., Fussl J., Griessner M. and Eberhardsteiner, J. (2014). Performance Assessment of a Numerical Simulation Tool for Wooden Boards with Knots by Means of Full-Field Deformation Measurements. *Strain*. **50**, pp.301317.

Levin, D. (2004). Mesh-Independent Surface Interpolation. *Geometric Modelling for Scientific Visualization*, Springer. pp.37-49.

Moore, A. (1991). *Efficient Memory based Learning for Robot Control*. PhD thesis, University of Cambridge.

Neagu, R.C., Gamstedt, E.K., Bardage, S.L. and Lindstrm M. (2006). Ul-

trastructural features affecting mechanical properties of wood fibres. *Wood Material Science and Engineering.* **1**, pp.146-170.

New Zealand Timber Industry Federation [online]. (2007). Available from: http://www.nzwood.co.nz/wp-content/uploads/2013/06/sawnmanufacture.pdf [**Accessed 4th January 2016**].

O'Sullivan, A.C. (1997). Cellulose: the structure slowly unravels. *Cellulose.* **4**, pp.173-207.

Sandberg, D. (2005). Distortion and visible crack formation in green and seasoned timber: influence of annual ring orientation in the cross section. *Holz als Roh- und Werkstoff.* **63**, pp.11-18.

Sandberg, K. and Salin, J. (2012). Liquid water absorption in dried Norway spruce timber measured with CT scanning and viewed as a percolation process. *Wood Science Technology.* **46**, pp.207-219.

Seeling, U. and Merforth, C. (2000). FRITS - a new equipment to measure distortion. *Holz als Roh- und Werkstoff.* **58**, pp.338-339.

Stone, J.E. and Scallan, A.M. (1967). Effect of component removal upon porous structure of cell wall of wood - 2. swelling in water and fibre saturation point. *Tappi.* **50**, pp.496-501.

Sun, S. and Salvaggio, C. (2013). Aerial 3D Building Detection and Mod-

elling From Airborne LiDAR Point Clouds. *IEEE Journal of Selected Topics in Applied Earth Observations and Remote Sensing.* **6**, pp.1440-1449.

Tagliasacchi, A. (2010). *MathWorks* [online]. Available from: http://uk.mathworks.com/matlabcentral/fileexchange/21512-kd-tree-for-matlab. [**Accessed 26th November 2013**].

Tiemann, H.D. (1906). *Effect of Moisture upon the Strength and Stiffness of Wood.* 1st. ed. Harvard University: U.S. Dept. of Agriculture, Forest Service.

Viscan [online]. (2016). Available from: http://microtec.eu/en/catalogue/products/viscan. [**Accessed 21st August 2016**].

Watt, M.S., Kimberley, M.O., Harrington, J.J., Riddell, M.J.C., Cown, D.J. and Moore, J.R. (2013). Differences in intra-tree variation in spiral grain angle for radiata pine. *New Zealand Journal of Forestry Science.* **43**, Article 12.

Weber, C., Hahmann, S. and Hagen, H. (2010). *Sharp Feature Detection in Point Clouds.* In: IEEE International Conference on Shape Modelling and Applications, 21-23 June 2010, Aix en Provence. pp. 175-186.

WoodEye [online]. (2016). Available from: http://woodeye.se/en/woodeye-5/. [**Accessed 2nd January 2016**].